Effect of CO_2 sequestration on long-term concrete performance and durability

Clinton Pereira and Rishi Gupta

2025

Original citation:
Pereira, C., & Gupta, R. (2025). Effect of CO2 sequestration on long-term concrete performance and durability. *Journal of Building Engineering*, *111*, 113553. https://doi.org/10.1016/j.jobe.2025.113553

Journal of Building Engineering 111 (2025) 113553

Contents lists available at ScienceDirect

Journal of Building Engineering

journal homepage: www.elsevier.com/locate/jobe

Effect of CO_2 sequestration on long-term concrete performance and durability

Clinton Pereira [a,b,c], Rishi Gupta [a,b,c,*]

[a] Department of Civil Engineering, University of Victoria (UVic), Canada
[b] Facility for Innovative Materials and Infrastructure Monitoring (FIMIM) UVic, Canada
[c] Centre for Advanced Materials and Related Technology (CAMTEC) UVic, Canada

ARTICLE INFO

Keywords:
CO_2 sequestration
Accelerated carbonation
Dynamic modulus
Corrosion resistance
Service life

ABSTRACT

As global greenhouse gas emissions have increased, all industries have been exploring green and sustainable materials and technologies. Studies have shown that adding CO_2 to concrete while it is mixed improves its hardened properties. This experimental approach aims to understand the impact of adding CO_2 during the mixing stage on the transport properties, freeze-thaw (F-T) resistance and corrosion resistance of embedded rebars. Key parameters like water permeability, rapid chloride ion penetration, resistivity, dynamic modulus, corrosion potential and rate were measured to assess the long-term durability. For CO_2 dosages ranging from 0.25 % to 1 % by weight of cement, a 50–90 % reduction in the permeability coefficient, a 25–40 % decrease in chloride ion penetration values, and a 10–20 % increase in resistivity were observed, in comparison to control. Additionally, CO_2 dosages between 0.5 % and 0.75 % showed improved resistance to F-T cycles, as observed by lower mass loss, less surface scaling, and increased stiffness. Concrete slab panels subjected to alternative wetting and drying cycles at elevated temperatures and salt-free environments showed improved corrosion resistance at CO_2 dosages between 0.5 % and 0.75 %. However, similar resistance could not be obtained in saline conditions, highlighting the need for supplementary protection to mitigate corrosion. This study also applies Tuutti's model to predict the service life of reinforced concrete to assess the effectiveness of CO_2 sequestration.

1. Introduction

Global temperatures have risen due to increased heat-trapping greenhouse gases (GHGs) in the atmosphere brought on by the overuse of natural resources, burning of fossil fuels, and deforestation [1]. The most critical anthropogenic contributor to GHGs is CO_2, which is produced in massive quantities [2]. It is a need of the hour to find a long-term solution to minimize the impact of CO_2 emissions on our environment globally [3]. All sectors are working towards minimizing their carbon footprint, and the construction industry has also been adopting ways to decarbonize and sequester CO_2 during the life cycle of structures [4]. Adding CO_2 during the mixing or curing stage of concrete have shown to improve certain properties [5–8]. However, as the natural carbonation process has led to carbonation-induced corrosion, doubts remain regarding the long-term durability of CO_2-sequestered concrete [9]. The extensive use of CO_2 sequestration in concrete by the construction industry is currently limited due to a lack of regulatory and codal

* Corresponding author. Department of Civil Engineering, University of Victoria (UVic), Canada
E-mail addresses: clintonpereira@uvic.ca (C. Pereira), guptar@uvic.ca (R. Gupta).

https://doi.org/10.1016/j.jobe.2025.113553
Received 13 March 2025; Received in revised form 22 June 2025; Accepted 21 July 2025
Available online 26 July 2025

approvals, insufficient field application data, and concerns about carbonation-induced corrosion in reinforced concrete structures. Although several studies have explored the plastic, mechanical and microstructural properties of CO_2-sequestered concrete, minimal research has been conducted to understand the effects of accelerated carbonation on concrete subjected to varying environmental conditions. Understanding these long-term effects has been the primary motivation for this study.

Researchers have highlighted that natural carbonation is a process by which concrete absorbs atmospheric CO_2 [10–14]. Marani et al. [15] explain that during this process, CO_2 enters the body of concrete through cracks and a network of interconnecting voids, drops the pH of the pore solution and destroys the passive protective layer leading to corrosion of the embedded rebars. Angst [16] describes that calcium hydroxide ($Ca(OH)_2$) formed in hydrated Portland cement pastes keeps the pH of concrete around 12.6, and the passive layer on the steel surface remains stable. When atmospheric CO_2 penetrates into concrete, calcium ions from hydrated cement paste react with aqueous CO_2 to form calcium carbonate ($CaCO_3$), as explained by Auroy et al. [5]. The pH of the pore solution can drop to around 9.0 when $Ca(OH)_2$ starts to reduce [14]. This is less than the de-passivation threshold of rebars which is around 9.5, as explained by Savija et al. [11], making the steel rebar vulnerable to corrosion. The corrosion process accelerates due to the presence of moisture and oxygen, which enter into the body of concrete through the network of cracks and interconnecting pores, which eventually lowers the life of the reinforced concrete structure [17]. Because of this, concrete is generally designed for low permeability and fewer cracks to stop the entry of water, CO_2 and other degrading chemicals into its microstructure and prevent corrosion of embedded rebars [18]. Alternatively, studies by Kamal et al. [7], Rostami et al. [19], Lagerblad [20], Shao [21], and Monkman et al. [22] have found that the strength and durability of concrete is increased when CO_2 is added during the mixing or curing process. Even though studies have demonstrated that CO_2 can be utilized to improve the properties of concrete, before implementing CO_2 sequestration as a sustainable building method, it is crucial to understand how it affects the long-term performance of concrete. To understand the long-term advantages and challenges of CO_2 sequestration in concrete, this literature review objectively examines transport characteristics, pH levels, freeze-thaw behaviour, and corrosion of steel in concrete based on prior studies.

1.1. Transport properties of concrete

Classie [23], highlights that transport properties of concrete determine its long-term durability. Concrete microstructure generally comprises of the solid, liquid, and vapour phases [24]. As detailed by Azarsa and Gupta [25], as the liquid phase contains pore water, the resistivity of this phase can be as low as 10 Ω-m. The authors also highlight that the solid phase, comprising of aggregates and hydrated cement paste, exhibits high electrical resistivity as high as 10^6 Ω-m. According to Li et al. [26], these properties govern the movement of water, CO_2 and salts of chlorides and sulphates and other deleterious material within the concrete mass, which eventually plays a crucial role in corrosion and cracking. Studies by Garboczi [27], Li et al. [28], Julio-Betancourt et al. [29], Feldman et al. [30], Spragg et al. [31], and Ramezanianpour et al. [32] have shown that minimizing surface cracks, reducing porosity and permeability, enhancing resistivity, minimizing chloride ion penetration and limiting sulphate attack, in addition to high strength, can improve the longevity and service life of reinforced concrete structures. Studies by Gupta [33] and Kamal et al. [34] have found that accelerated carbonation densifies the concrete matrix and reduces permeability, while Elkhaldi et al. [35] observed higher electrical resistivity. Additionally, a decrease in the porosity of concrete was observed by Gil et al. [36] and Kazemian et al. [37] in concrete subjected to early-age carbonation. Although several studies have been conducted on the transport properties of CO_2-sequestered concrete, there is still a research gap on the impact of these properties on the long-term durability of concrete under varying environmental conditions. The impact of reduction in porosity, permeability, and increased resistivity on freeze-thaw resistance of concrete also remains unexplored.

1.2. Freeze-thaw resistance of concrete

Extensive research has been done to date to understand the resilience of concrete to Freeze-Thaw (F-T) cycles. According to Zhao et al. [37] and Cai and Liu [38], F-T damage of concrete takes place due to the freezing and thawing of water trapped within the pore structure of concrete. As per ACI Committee, 201.2R-16 [39], using air-entraining agents improves the F-T resistance of concrete by allowing the freezing water inside it a space to expand. According to Auroy et al. [5] and Monkman et al. [22], when concrete is sequestered with CO_2, the carbonation reactions decrease the porosity of concrete, which in turn reduces the freezable water in the pores and eventually minimizes the pressure build-up from inside. On the other hand, Kamal et al. [7] and Savija et al. [11] point out that the carbonation process might reduce porosity, which leaves concrete vulnerable to F-T damage. The impact of adding CO_2 to concrete during the mixing stage on its F-T resistance needs to be better understood experimentally in order to answer the concerns expressed by some researchers.

1.3. pH of concrete

According to Fajardo et al. [40] and Shaheen and Pradhan [41], the passive layer formed on the surface of rebars remains stable due to the highly alkaline environment of concrete and protects the steel bars against corrosion. The pore solution in concrete is usually between 12.5 and 13.5, as referenced in the research by Silva [42]. Concrete starts losing its alkalinity when $Ca(OH)_2$ starts reducing while getting converted to $CaCO_3$ during carbonation [14]. According to Savija et al. [11], the consumption of $Ca(OH)_2$ lowers its pH, which slowly removes the protective layer on the steel reinforcement and increases the likelihood of corrosion. Scholars like Guo et al. [43] and Steffens et al. [44] support the argument that this pH reduction can seriously jeopardize the durability of reinforced concrete. These conclusions by some researchers set the ground for additional work required to determine the impact of adding CO_2 during the

mixing stage of concrete on its pH levels and understand its effects in protecting the steel reinforcement from carbonation-induced corrosion.

1.4. Corrosion of steel in concrete

Since steel reinforcement is used in most concrete constructions, Talukdar and Banthia [45] highlight the importance of understanding the effect of carbonation on steel rebars to assess the long-term durability and service life of reinforced concrete structures. Chlorides can break down the passive protective layer on the steel surface even at high pH, and the combination of carbonation and chloride penetration can accelerate corrosion [46]. Research by Gupta [33], Guo et al. [43], and Kamal et al. [34] has highlighted that when CO_2 is added to concrete during the mixing stage, the microstructure of concrete is densified, and durability is increased; however, their study does not analyze its impact on the corrosion of rebars. Furthermore, limited research has been done to study the impact of elevated temperatures and salt solution on embedded rebars in CO_2-sequestered concrete. To address this gap, this study has conducted a few expedited tests with harsh environmental conditions.

This overview of literature aligns with this experimental study on the long-term effects of CO_2 sequestration in concrete. Studies by several researchers have indicated that adding CO_2 to concrete during the mixing stage has provided benefits and some challenges. However, due to insufficient experimental data on the long-term effects of CO_2 sequestration in concrete, the construction industry is skeptical of the implementation of this technology. To fill in these gaps on this subject and assess the impact of early-age carbonation on long-term durability, this study first analyzes the impact of adding CO_2 during the mixing stage on the transport properties of concrete and the impact of densification on the concrete microstructure. It further studies its resistance to deterioration when subjected to 300 F-T cycles, with an aim to identify the effect of early-age carbonation on the frost action of concrete. Lastly, it aims to understand the effect of CO_2 addition on the resistance of concrete to carbonation and chloride-induced corrosion when subjected to harsh environmental conditions of alternative wetting and drying cycles at elevated temperatures, with and without the presence of corrosive salts. By expanding on the work from previous researchers and filling some of the knowledge gaps, this experimental work aims to provide the concrete industry with helpful information which can be used for implementing CO_2 sequestration in concrete during the mixing stage. The conclusions from this study will offer important guidance on implementing this technology without sacrificing the sustainability and structural soundness of concrete structures.

2. Methodology

2.1. Raw materials, concrete mix design and CO_2 sequestration process

Portland Limestone Cement (PLC), conforming to the CSA A3001-03 GUL (General Use Limestone) standard [47] or ASTM C595 for Type IL [48] (PLC with up to 15 % limestone content) was used. Natural sand and crushed granite locally sourced and meeting ASTM C33/C33M − 18 [49] specifications were used. A superplasticizer, based on polycarboxylate technology meeting with Type F requirements of ASTM C494/C494M − 19 [50] was used. Additionally, an air-entraining admixture (AEA) meeting ASTM C260-10 [51] standards was utilized, to provide 6 % air content in the concrete mix.

A 40 MPa concrete mix was designed following the ACI PRC-211.1-91 [52] guidelines for proportioning normal, heavyweight, and mass concrete. The mix was designed to meet C2, S2, and A2 class exposure conditions according to the Canadian Standards Association (CSA A23.1:24) [53]. Detailed mix proportions for the 40 MPa concrete are provided in Table 1. Sample preparation adhered to ASTM C192/C192M − 19 [54] procedures using a tilting drum mechanical mixer. Dry ingredients were mixed for 2 min, followed by 3 min of wet mixing. Superplasticizer and AEA were added to the mixing water.

For CO_2-sequestered concrete, CO_2 gas was injected after the initial wet mixing phase. The pure industrial-grade CO_2 gas cylinder was sourced from a certified gas supplier (99.8 % purity) [55]. A regulator and a flowmeter was connected to the cylinder to accurately control the CO_2 flow rate in cubic feet per hour (CFH) and duration in minutes. Gas loss during mixing was minimized using a wooden lid, clamps, and a rotating copper pipe with a flexible hose to the drum mixer, including full submersion of the copper pipe in the mix for uniform gas dispersion. The amount of CO_2 injected was calculated based on the dosage levels (0.25 %, 0.5 %, 0.75 %, and 1 % by weight of cement), derived from the ideal gas law. For the CO_2-sequestered concrete mixes an additional dosing and mixing time ranged from 2 to 6 min to achieve proper dosing and uniform distribution of CO_2 within the concrete. A 1 % dosage limit was

Table 1
Concrete mix design.

Concrete Ingredients	Grade 40 MPa
Cement (kg/m^3)	400
Water (kg/m^3)	160
water/cement ratio	0.4
Fine aggregate (kg/m^3)	712
Coarse aggregate (9.5 mm) (kg/m^3)	464
Coarse aggregate (19 mm) (kg/m^3)	567
Superplasticizer (% bwc)	0.3
Air Entraining Admixture (%bwc)	0.3
Theoretical bulk density (kg/m^3)	2305

established based on set of multiple trials [56] and literature [57–59], which indicated that exceeding this amount negatively affected workability and slump, justifying the threshold to maintain balance between improved concrete performance and ease with which concrete can be placed and finished in its final location.

As explained by Lagerblad [20], $Ca(OH)_2$ from the hydrating cement reacts directly with CO_2, leading to the formation of $CaCO_3$. The author further highlights that water is needed in its transformation, which results in a drop in the workability of the concrete mix. To counteract the slump reduction due to CO_2 exposure, an additional dose of superplasticizer, ranging from 0.1 to 0.3 % by weight of cement (bwc), was added to maintain a slump of 125–150 mm during casting, with an additional 1 min of mixing time. This additional CO_2 dosing and mixing time may have also been the reasons for the reduction in the workability of concrete observed in the CO_2-sequestered concrete mixes. Lab conditions were at 15 ± 5 °C and 65 ± 5 % relative humidity during the mixing and casting process. After 24 h of casting, the samples were cured in a tank at 23 ± 2 °C until testing. Compressive strength testing was conducted at 7, 28, and 90 days in accordance with ASTM C39-21 [60]. The tests utilized a compression testing machine with a 2000 KN load capacity, applying the load at a stress rate of 0.25 MPa/s ± 0.05 MPa/s.

Details about the raw material properties, mix proportioning, CO_2 sequestration process, plastic and mechanical properties, and microstructural investigation, focusing on the hydration, structure, and strength of CO_2-sequestered concrete, can be found in the other published work by the authors of this paper [56].

2.2. Transport properties of concrete

2.2.1. Surface electrical resistivity test

According to AASHTO 358-19 [61], the surface electrical resistivity test uses the four-probe (Wenner-Array) approach to measure the resistivity on the concrete surface. As shown in Fig. 1(a), this test was conducted on the surface of a cylindrical specimen measuring 100 × 200 mm at 28 days. The test procedure, as explained in AASHTO 358-19, was followed. The specimens were kept submerged in water maintained at 23 ± 2 °C before the test and tested under SSD conditions after 28 days of casting. This instrument measured resistivity along the curved face of the cylindrical concrete specimen using four channels of a 4-probe array, positioned at 90° intervals from each other [62]. As per the manufacturer, it records the resistivity based on an average of eight sets of measurements. The measuring device, built with a data acquisition system (DAQ), passes a current between the outer two electrodes, while the voltage is measured between the inner two electrodes [63].

2.2.2. Rapid Chloride Permeability Test

The Rapid Chloride Permeability Test (RCPT), an indirect measure of the durability of concrete under chloride attack, was used to measure the chloride ion penetration [30]. In compliance with ASTM C1202-22 [64], the test was carried out following 28 days of water curing; however, AASHTO T277 [65] or any other applicable standard may also be utilized. Following the procedure as explained in ASTM C1202-22, three samples of each CO_2-sequestered concrete mix were made for the test. Two specimens of 50 mm thickness were cut from each 100 × 200 mm cylinder. The curved faces of the cylindrical specimens were sealed with waterproof tape to prevent leakage of water, which could compromise the test results. The samples were submerged in water for 20 h after 3 h of low-pressure (less than 50 mm Hg) vacuum desiccator treatment. Before starting the RCPT test, the instrument was calibrated using a verification kit provided by the manufacturer [66]. In accordance with the ASTM C1202-22 standard, the test runs for 6 h, and the device automatically recorded the current flowing through the material at regular intervals, using the measuring device inbuilt with a DAQ, as shown in Fig. 1(b) [67]. This test links the total electrical charge that flows through the material, measured in Coulombs, to provide an indirect indicator of the permeability of concrete to chloride ions. The chloride ion penetration can be classified into the categories as provided in Table 2 in accordance with ASTM C 1202-22.

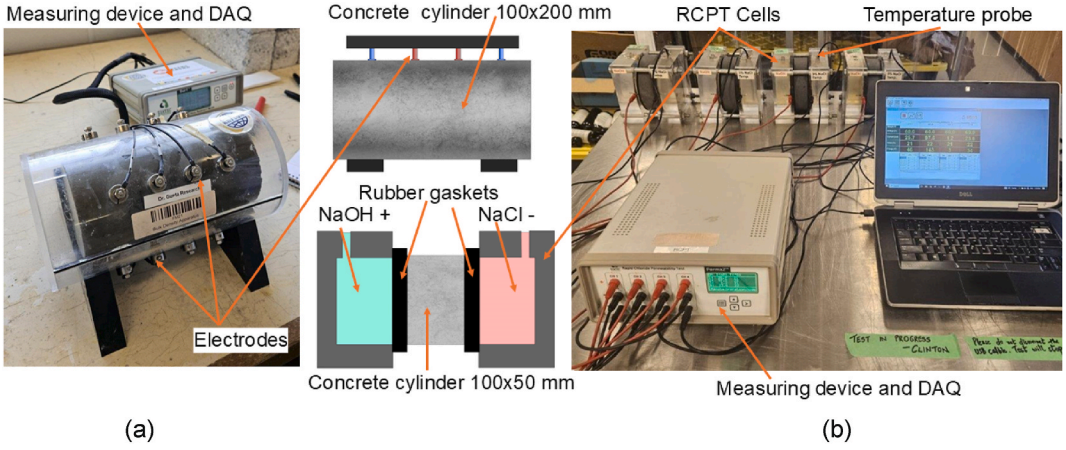

Fig. 1. (a) Surface electrical resistivity test and (b) rapid chloride permeability test.

2.2.3. Water permeability test

In order to measure the resistance of concrete to the movement of water, chemicals and salts within its pore structure, the water permeability test is usually conducted [10]. This test is typically conducted following the procedures outlined in BS EN 12390–8:2019, DIN 1048-5, or other relevant standards. For this particular test, BS EN 12390–8:2019 [68] standard was followed. Three cubic specimens with 150 mm sides that were cast and cured for 28 days in accordance with ASTM C192/C192M − 19 [54]. The specimens were mounted on the water permeability apparatus, with the formed surface in contact with the water inlet at the bottom to prevent any water leakage. During the test, the pressure was maintained at 500 ± 50 kPa, creating a water head of 51 m (H). This pressure was maintained for 72 h (t), after which the specimens were split in half using a cube splitting jig, and water penetration depth was immediately marked and measured.

The coefficient of permeability (k) is generally calculated using the depth of water penetration, as explained by Mehta and Monterio [69]. The coefficient of permeability (k) is determined using Darcy's law, as shown in equation (1), where dq/dt is the rate of water flow, μ is the viscosity of water, ΔP is the pressure gradient, A is the surface area, and L is the thickness of concrete.

$$\frac{dq}{dt} = k\,\frac{\Delta P\, A}{L\mu} \tag{1}$$

Equation (2) describes the model that Ibrahim and Issa [70] suggested to estimate the permeability coefficient based on the average depth of water penetration. In this model, C represents the ratio of the average to the maximum water penetration depth ($d_{average}/d_{max}$), t is the test duration (seconds), and H is the hydrostatic head driving the water percolation (m).

$$k = C^2 \frac{d^2\, max}{Ht} \tag{2}$$

2.2.4. Scanning electron microscopy imaging

The microstructural differences in porosity between CO_2-sequestered concrete and a control concrete sample was evaluated using a tabletop scanning electron microscope (SEM). The Hitachi TM4000 Plus tabletop SEM was used in low magnification mode (30x). The test was conducted after 90 days of curing to ensure complete hydration and concrete samples incorporating CO_2 had sufficient time for early age carbonation processes to take place. Cylindrical specimens with 0 %, 0.5 %, and 1 % CO_2 dosages were sectioned into thin slices approximately 2–3 mm thick using a diamond saw. These slices were subsequently polished using a polishing machine and abrasive papers of 500, 1500, and 2500 grit, each for around 2–3 min under water. From each polished slice, small prismatic samples measuring roughly 2 × 2 × 2 mm were extracted. These samples were cleaned and oven-dried at 110 ± 5 °C for 24 h to eliminate residual moisture. For SEM analysis, the dried specimens were affixed to stubs using conductive copper tape to ensure effective electrical grounding, preventing surface charging during imaging of the non-conductive concrete matrix. Prior to imaging, the mounted samples were subjected to a 24-h cleaning cycle in a Hitachi zone cleaner, which utilized UV light and vacuum to remove surface hydrocarbons and other contaminants. The samples were then analyzed in backscattered electron (BSE) mode to examine the presence of microvoids in low magnification mode (30x).

2.3. Freeze-thaw testing of concrete

For each concrete batch, three 75 x 100 × 405 mm specimens were cast for different CO_2 dosages (0 %,0.25 %,0.5 %,0.75 % and 1 %) and cured as per ASTM C192-19 [54], for a period of 28 days after casting. These specimens were subjected to standard cyclic F-T testing up to 300 cycles as per ASTM C666-15 [71], Procedure A (Rapid Freezing and Thawing in Water) without de-icer salts. A Humboldt HC-3186S·4F freeze-thaw cabinet was used for the test. As summarized in the operation manual provided by Humboldt Mfg. Co [72], a 0.75 HP (0.6 KW) refrigeration unit and electric resistance heaters with fully automated controls were used to maintain the temperature of the concrete prisms. The specimens' temperatures were lowered from 4 to −18 °C and raised from −18 to 4 °C over the course of roughly 3.5 h in each F-T cycle, in accordance with the procedure explained in ASTM C666-15. As suggested by the manufacturer of the F-T cabinet, to ensure an automatic cyclic F-T temperature control by the machine, a thermocouple was placed in the middle of the control specimen. Additionally, using metallic spacers, the specimens in the F-T moulds were fully submerged in 1–3 mm of water during the test, ensuring water contact throughout the freezing-thawing cycles. As per the procedure explained in ASTM C666-15, non-destructive testing (NDT) methods were used to determine the fundamental transverse, longitudinal, and torsional frequencies, in addition to surface resistivity, and ultrasonic pulse velocity (UPV), including mass loss measurements at intervals of 0, 30, 60, 90, 120, 150, 180, 210, 240, 270, and 300 F-T cycles. All tests were performed on specimens in a saturated surface dry (SSD) condition at a room temperature of 23 ± 2 °C. Because the relative dynamic modulus of elasticity did not decrease below 60 % of the

Table 2
Chloride Ion permeability based on charge passed.

Charge passed (Coulombs)	Chloride ion penetrability
>4000	High
2000–4000	Moderate
1000–2000	Low
100–1000	Very low
<100	Negligible

initial modulus, the test continued up to 300 cycles as stipulated by ASTM C666-15.

2.3.1. Mass loss

The percent mass loss at various F-T cycles was recorded to assess the durability and resistance of the concrete to freeze-thaw damage. The mass loss rate is described in equation (3).

$$\Delta Wn = \frac{(W0 - Wn)}{W0} \text{ x100} \tag{3}$$

Where ΔW_n is the mass loss rate after n F-T cycles (%), W_0 is the mass at 0 F-T cycle (kg), and W_n is the mass after n F-T cycles (kg).

2.3.2. Resonance frequency

The longitudinal, transverse, and torsional fundamental frequencies were measured using resonance frequency testing as per the procedure explained in ASTM C215-19 [73] to determine the durability factor and dynamic modulus of CO_2-sequestered concrete and compare it with control concrete to observe changes in physical properties. This study utilized a resonance test gauge by Olson Instruments with a built-in data acquisition system and a PCB Piezotronics accelerometer. The manufacturer of this instrument provided a 110 g steel ball peen hammer that could produce resonance frequencies up to around 10 kHz when struck on a flat concrete surface with a light force. According to the procedure explained in ASTM C215-19 [73] for the impact resonance method, the accelerometer was placed intact on the concrete surface using a petroleum gel, and the concrete specimen was struck with a hammer to determine the fundamental longitudinal, transverse, and torsional frequencies. The test was repeated for each specimen after every 30 F-T cycles from 0 to 300 cycles. ASTM C215-19 specifies the procedure to determine the dynamic elastic and rigidity modulus based on the resonant frequencies of the specimens. Equation (4) was used to calculate the dynamic Young's modulus of elasticity (E) from the fundamental transverse frequency; equation (5) was used to calculate the dynamic Young's modulus of elasticity (E) from the fundamental longitudinal frequency, and equation (6) was used to determine the dynamic modulus of rigidity (G) from the fundamental torsional frequency, as provided by ASTM C215-19.

$$\text{Dynamic E} = \text{C x M x n}^2 \tag{4}$$

$$\text{Dynamic E} = \text{D x M x } \left(n^{I}\right)^2 \tag{5}$$

$$\text{Dynamic G} = \text{B x M x } \left(n^{II}\right)^2 \tag{6}$$

Where C, D and B are dimensional factors of the specimen, M is the mass of the specimen, and n, n^I, n^{ll} represent the fundamental transverse, longitudinal and torsional frequency, respectively, after c cycles of freezing and thawing.

2.3.3. Ultrasonic pulse velocity

Concrete quality and consistency can be assessed non-destructively using Ultrasonic Pulse Velocity (UPV) testing ASTM C597-22 [74]. As explained by Mohana [75], this test is established using the pulse velocity method to obtain information regarding the uniformity of concrete and identify any cracks, cavities, and other defects. The author further explains that because of these defects inside concrete, the travel path of the waves becomes blocked, increasing their travel time and decreasing their velocity. A Proceq Pundit Lab UPV test apparatus, which included two 50 mm diameter transducers and an electrical pulse generator operating at 54 kHz, was utilized to test the concrete prisms for UPV. To ensure adequate contact between the transducers and the concrete surface, cellulose gel was applied to the surface of the transducers in contact with the concrete surface. Following the procedure outlined in ASTM C597-22 [74], the UPV testing was carried out. The test was carried out on the formed surface of the concrete prisms in both longitudinal and transverse directions for each specimen utilizing a direct transmission mechanism. The pulse velocity in m/s is given by equation (7).

$$V = L/T \tag{7}$$

Where, V is the longitudinal pulse velocity, L is the path length, and T is the time taken by the pulse to traverse that length.

The dynamic modulus of elasticity (Ed) was derived from the UPV test, which was calculated using the velocity of the ultrasonic pulse passing through the concrete and its density, as explained by IAEA guidelines [76]. The relationship between the pulse velocity, density and dynamic Poisson's ratio is given by equation (8).

$$Ed = \left(\rho\, V2\, \left[\frac{(1+\upsilon)(1-2\upsilon)}{1-\upsilon}\right]\right) \tag{8}$$

Where, Ed is the dynamic elastic modulus, ρ is the density of concrete, V is the pulse velocity, and υ is the dynamic Poisson's ratio. A Poisson's ratio of 0.2 was used for the calculation of dynamic modulus referring to the study by Swamy [77]

2.3.4. Resistivity

The resistivity of concrete was measured in accordance with AASTHO T358-19 [61], this test makes use of a Wenner 4 probe to provide the surface electrical resistivity of concrete.

2.4. pH of concrete

To determine if there were any changes to the alkalinity of concrete after CO_2 sequestration, pH measurements were done. The indirect pH measurement was done by mixing powdered concrete samples with distilled water. After testing the cylindrical specimens for 90-day strength, one cylinder was broken into smaller pieces using a hammer and placed in an oven at 110 ± 5 °C for 24 h to dry free water. The concrete samples were then crushed into a fine powder using an automatic Marshall impact compactor, and the powder was sieved by a 90-μm sieve. As per the procedure detailed by Robayo-Salazar et al. [14],15 g of the concrete powder was mixed with 150 g of distilled water and mixed on a magnetic plate for 20 min. After mixing, the pH values of each suspension were measured three times using a digital pH meter. The qualitative analysis was experimentally done by splitting the concrete cylinders in half, spraying a 1 % phenolphthalein solution on the concrete surface, and observing the colour change.

2.5. Evaluation of corrosion resistance of reinforced concrete

The alternate wetting and drying cycle test was conducted to check the resistance of CO_2-sequestered concrete to withstand corrosion. The test was performed both with and without the addition of chloride salts. In order to estimate the service life and provide information about its long-term performance, the Tuutti Model [78] was also utilized. Concrete slab panels measuring 300 x 300 × 100 mm were cast, each containing four deformed low-carbon steel reinforcement bars of 10 mm diameter, conforming to CSA G30.18 [170]. The bars were arranged in a crosswise pattern in a wooden mould, as illustrated in Fig. 2(a), to simulate typical reinforced concrete slab conditions. As shown in the schematic sketch in Fig. 2(b), 4 bars, each 240 mm in length, were placed crosswise with a 60 mm spacing between the four nodes. The ICOR (instantaneous corrosion) rate measurement equipment of Giatec Scientific Inc. was used, which has an electrode influence area with a diameter of 180 mm. The rebar mesh spacing was designed in such a way that the four nodes of the rebars aligned with the electrodes of the ICOR device. A clear cover of 30 mm was provided to the bottom steel, in accordance with CSA A 23.1 requirements, by using plastic spacers as indicated in Fig. 2(a). The rebars were designed with a length that ensured a minimum concrete cover of 30 mm in all directions within the slab. To conduct half-cell potential measurements, an electrical copper wire was connected to one rebar, which was also in contact with the other three rebars. Panels were cast for each of the five mixes, with CO_2 dosages ranging from 0 % to 1 %. After the concrete was poured into the wooden moulds, it was compacted by placing them on a vibrating table. After 24 h of casting, the slab panels were demoulded and cured for 28 days in a controlled lab environment at 23 ± 2 °C. During this period the panels were covered with moist hessian cloth to maintain a humid environment and prevent moisture loss from concrete.

After 28 days of water curing, each slab panel was tested under alternating wetting and drying conditions following the procedure outlined by Elbakari and Shehata [79]. The wetting-drying cycle for this test consisted of 50 cycles over 100 days. Rangel et al. [80] implemented 50 wetting-drying cycles over a 100-day period to replicate conditions, such as heavy rainfall and hot summers, in the laboratory. This approach ensured that the impact of alternating wetting and drying conditions could be evaluated across the different slab panels with varying CO_2 dosages. The test was performed manually with the use of water tubs and laboratory ovens. Sets A, B and C comprised of five slab panels each, with CO_2 dosages ranging from 0 % to 1 %, subjected to wetting and drying exposure conditions as detailed in Table 3. Each cycle lasted for 24 h, ensuring both complete drying of water present in the concrete pores in the drying cycle and saturation of concrete in the wetting cycle. The slab panels in set A were placed in the oven set at to 50 °C, and panels in sets B and C were subjected to 60 °C. Sets A and C had their wetting cycle in potable water, whereas Set B had the wetting cycle in potable water with 5 % NaCl concentration. All tests were conducted at the 0th and at the end of the 25th and 50th, as per the timelines indicated in Fig. 3. An ICOR device, a half-cell potential copper-copper sulphate electrode, and a Wenner four-probe resistivity measurement equipment were used to measure the corrosion rate, corrosion potential and the resistivity of concrete, respectively. The ICOR device was used to record the concrete resistivity and corrosion rate readings at each node in both horizontal and vertical locations. Additionally, a Wenner four-probe instrument was used to test resistivity in each of the four quadrants in the slab.

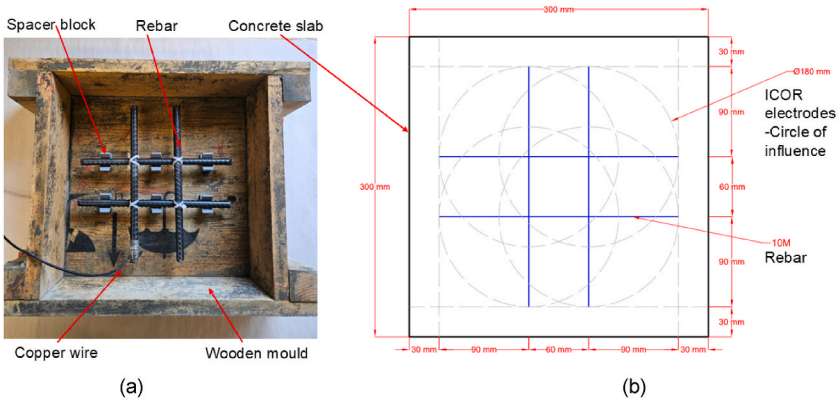

Fig. 2. (a) Rebar layout for corrosion testing, and (b) Schematic sketch of rebar design in the slab.

Table 3
Wetting and drying exposure conditions.

Category	Wetting cycle (Water temp- 23 ± 2 °C)	Drying cycle (Oven temp)
Set A	Potable water	50 °C
Set B	Potable Water+ 5 % NaCl	60 °C
Set C	Potable water	60 °C

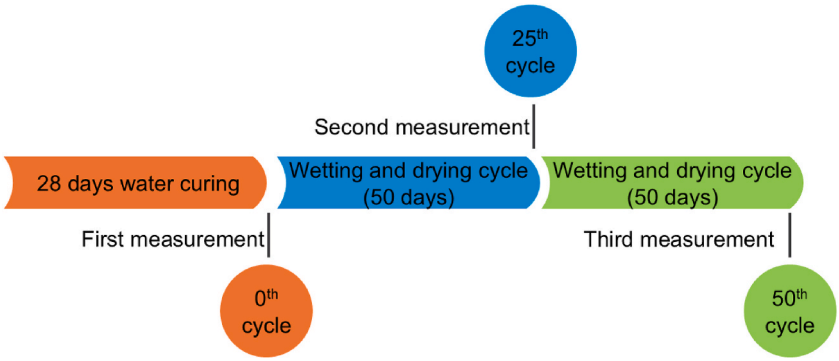

Fig. 3. Wetting and drying cycle testing regime.

2.5.1. Corrosion rate measurement

In this test, the corrosion rate of the steel rebar in concrete was measured using the non-destructive ICOR instrument by Giatec Scientific Inc. [81]. It functions according to the linear polarization resistance (LPR) concept. As explained by the manufacturer [82], the device has a four-probe Wenner array design, where a steady AC current is delivered between the outer probes and voltage measurements are obtained between the inner probes. The rebars in the samples were identified and marked using a rebar locator to pinpoint the four nodes, as shown in Fig. 4(a). Furthermore, Fig. 4(b) shows the positioning of the ICOR device at the nodes on the concrete slab for corrosion rate measurements and resistivity. These measurements were taken every 30 min at each of the four nodes, as recommended by the manufacturer. As the circle of influence for the four nodes overlaps, repeated measurements can cause residual polarization effects to occur at the rebar surface, which can lead to inaccurate results of corrosion rate or current density. The instrument was calibrated to provide the corrosion rate of rebar in micro-Amps per square centimetre ($\mu A/cm^2$) and the corrosion penetration rate in μm/year.

2.5.2. Half-cell potential test

To measure the corrosion potential of steel rebars embedded in the 300 × 300 × 100 mm concrete slab panels, a copper-copper sulphate (Cu-$CuSO_4$) electrode, a digital multimeter and a wire connected to the rebar mesh were used as shown in Fig. 4(c), following the procedure as described in ASTM C876-15 [83]. The voltage readings for each slab panel in sets A, B and C were recorded at the 0th cycle and at the end of the 25th and 50th cycle. To ensure proper coverage of the electrode base over all four overlapping bars

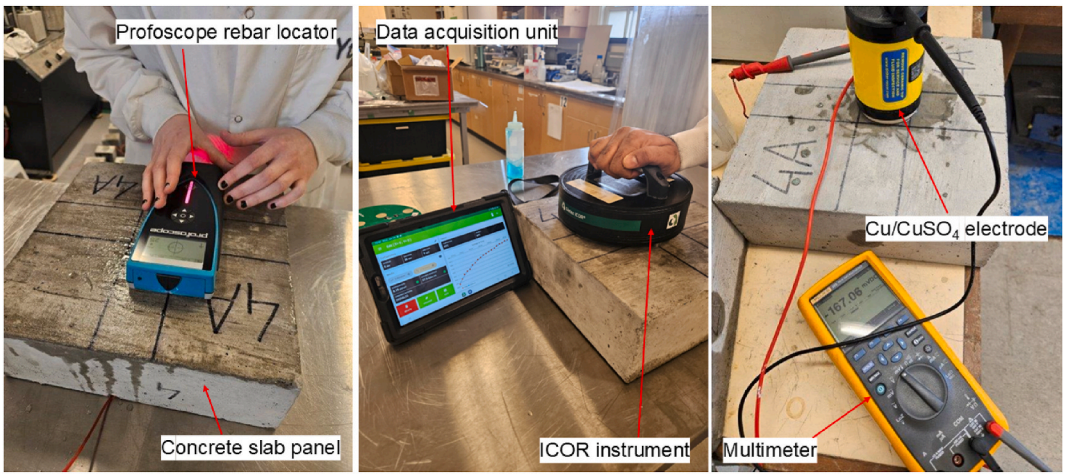

Fig. 4. (a) Rebar locator, (b) ICOR measuring device and (c) Half cell potential test set-up.

at the center of the slab, where the bar spacing is 60 mm center-to-center, a 75 mm diameter waffle-patterned, pre-calibrated electrode was used. The concrete surface in contact with the electrode was made moist with water to ensure good conductivity. The voltage value was recorded once the reading stabilized to within ±0.02 V, as per ASTM C876-15.

3. Results and discussions

The long-term performance and durability of CO_2-sequestered concrete are discussed in this section, with an emphasis on transport properties, freeze-thaw behaviour, pH of concrete and corrosion resistance. A comparison has been done between CO_2 sequestered concrete specimens and control concrete to understand the benefits, if any. In a previous publication by the authors of this study [56], the plastic, mechanical and microstructural properties of CO_2 sequestered concrete were evaluated and compared with control concrete. Compressive strength results showed 10–20 % improvement in both 25 MPa and 40 MPa concretes for CO_2 dosages of 0.5–0.75 %, with 0.75 % achieving the highest strength at all ages. Enhanced dry density confirmed densification of the matrix. Flexural and split tensile strengths showed an improvement of 5–10 % at 0.5–0.75 % CO_2 dosages, reinforcing the hypothesis that moderate CO_2 dosing enhances concrete mechanical properties. CO_2 injection during mixing reduced slump significantly across dosages above 0.5 %, as compared to the control mix. To ease placement of concrete in the moulds the slump/workability of the mix was rectified by adding a higher dosage of the superplasticizer. This effect was mainly due to the chemical reactions involved, increase in the heat of hydration and additional mixing times during CO_2 injection. The increase in heat of hydration was validated through the semi-adiabatic calorimetry test which revealed higher heat release in mixes with 0.75 % and 1 % CO_2 dosage, as compared to the control concrete mix. This heat release was attributed to the formation of $CaCO_3$, which also contributed to the densification of hardened concrete. Additionally the thermal pyrolysis test, SEM and Energy Dispersive X-ray Spectroscopy (EDX) analysis and Fourier Transform Infrared (FTIR) spectroscopy analysis indicated the formation of $CaCO_3$ in CO_2 sequestered concrete mixes, thereby confirming the carbonation reactions.

3.1. Transport properties of concrete

3.1.1. Surface electrical resistivity, RCPT and water permeability

The surface electrical resistivity and RCPT test results are graphically represented in Fig. 5(a) and (b), and the water permeability test results and computed coefficient of permeability are compiled in Table 4. The RCPT values are the average of three cylindrical specimens, while the resistivity test data are the mean of six cylinders. The error bars on the bar graphs indicate the standard deviation.

From Fig. 5 and Tables 4 and it can be observed that the control concrete sample shows the highest permeability and RCPT values and comparatively lower resistivity than other dosages of CO_2 addition. Further reduction in permeability was observed at 0.50 % CO_2 dosage, indicating better resistance to the flow of water and other deleterious materials. At 0.75 % the permeability and RCPT were comparatively low, and the resistivity was higher as compared to other CO_2 dosages, indicating improvement in durability due to the densification of the matrix. All the concrete samples indicate a low chloride ion permeability value in accordance with ASTM C1202-22 criteria, as summarized in Table 2.

At 1 % CO_2 dosage, the resistivity and permeability values were lower as compared to the 0.75 % CO_2 dosage indicating a threshold in early age carbonation benefits. Higher CO_2, above 0.5 % dosages reduced slump as observed in the concrete trials and plastic properties, found in the other published work by the authors of this paper [56]. This made the concrete harder to compact, potentially leading to entrapped air, and increased microvoids. As highlighted by Lagerblad [20], at high CO_2 dosages carbonation reactions may extend beyond calcium hydroxide ($Ca(OH)_2$) and begin to react with the calcium silicate hydrate and result in microstructural weakening. The authors of this study hypothesize that the observed reduction in resistivity and increase in permeability at the 1 % CO_2 dosage indicate that carbonation reactions exceeded the optimal limit. Additionally, the increased entrapped air and microvoids and microstructural damage led to a reduction in performance achieved at 0.75 % CO_2 dosage.

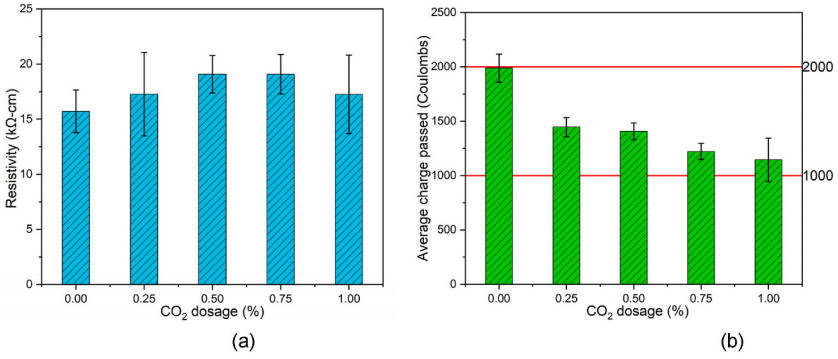

Fig. 5. (a) Average surface electrical resistivity, and (b) RCPT-Average charge passed in Coulombs.

Table 4
Coefficient of permeability (k) m/s.

Water permeability test					
Particulars	Control	0.25 %	0.50 %	0.75 %	1.00 %
$d_{average}$ (m)	0.02	0.01	0.01	0.01	0.01
$d_{std.dev}$ (m)	0.0015	0.0015	0.0026	0.0010	0.0006
d_{max} (m)	0.02	0.02	0.01	0.01	0.01
C	0.92	0.91	0.70	0.83	0.95
2 HT (m s)	26438400				
k (m/s)	1.41×10^{-11}	7.06×10^{-12}	1.85×10^{-12}	9.46×10^{-13}	1.68×10^{-12}

3.1.2. SEM imaging analysis

SEM images were captured in backscattered electron (BSE) mode at 30 × magnification to maintain consistent resolution and contrast across all samples. Fig. 6(a), (b) and 6(c) show the SEM images of 0 %, 0.5 % and 1 % CO_2 dosage samples, respectively, after 90 days of curing. The air voids appear dark in the SEM images due to low atomic density. The SEM imaging of the three samples indicates a reduction of voids in the concrete microstructure for the CO_2-sequestered concrete samples as compared to the control concrete sample, which confirms the densification effect.

A Java-based image processing software, ImageJ, was used to measure the percentage of air voids from the SEM images shown in Fig. 6. The images were converted to a grayscale using the binary function in the ImageJ software, where the threshold was set to isolate dark regions representing air voids. To maintain consistency, the same threshold settings were applied across all images. The data from ImageJ, summarized in Table 5, for the three CO_2 dosages (0 %, 0.5 %, and 1 %) provides insights into the void distribution in concrete at the microstructural level. 274 voids were identified in the control concrete specimen as compared to 72 and 24 voids, respectively, in the concrete specimens with 0.5 % and 1 % dosage. This reduction in the void count results from the densification of the microstructure due to early-age carbonation. Furthermore, the void area has been found to decrease with 0.062 mm^2 for 0.5 % and 0.048 mm^2 for 1 % dosage, compared to 0.238 mm^2 for control concrete. Additionally, the void region accounts for 1.813 % of the entire picture area for the control concrete specimen, as compared to 0.46 % and 0.35 % for 0.5 % and 1 % CO_2 dosage respectively, indicating a reduction in porosity. This analysis strengthens our hypothesis that adding CO_2 to concrete during the mixing stage leads to the densification of its microstructure.

3.1.3. Statistical analysis of transport properties

To determine if a correlation exists between permeability, RCPT charge passed, and concrete resistivity, a statistical analysis was conducted. The test outcomes are shown in Table 6, along with the Pearson correlation coefficient values for the above-mentioned pairs, determined using the Microsoft Excel data analysis tool. The Pearson correlation coefficients have been interpreted by referring to the article by Schober et al. [84]. The very strong positive linear relationship between the coefficient of permeability and chloride ion penetration from RCPT indicates that adding CO_2 to concrete helps to minimize both these parameters and eventually enhances durability. The moderately strong to strong negative linear connections between RCPT and resistivity and the coefficient of permeability and resistivity, respectively, indicate that the resistivity of concrete is influenced by some other factors. Both the experimental data and the Pearson coefficients support the hypothesis that adding CO_2 to concrete during the mixing process improves its durability.

The comparison of transport properties of both control and CO_2 sequestered concrete, which includes surface electrical resistivity, rapid chloride penetration (RCPT), and water permeability, confirms that early-age carbonation improves the durability of concrete, up to an optimal dosage threshold between 0.5 % and 0.75 %. Additionally, the SEM imaging and analysis of air void count and area indicates microstructural densification at the microscopic level. Conversely, at a 1 % CO_2 dosage, a decrease in resistivity and an increase in permeability was observed, suggesting that higher CO2 dosages can adversely durability of concrete due to over reaction of calcium ions from $Ca(OH)_2$ and C-S-H causing microstructural instability and increase in voids due to loss of workability. The findings from the tests on transport properties of concrete highlight a threshold in CO_2 dosages for early age carbonation, beyond which carbonation benefits start to diminish.

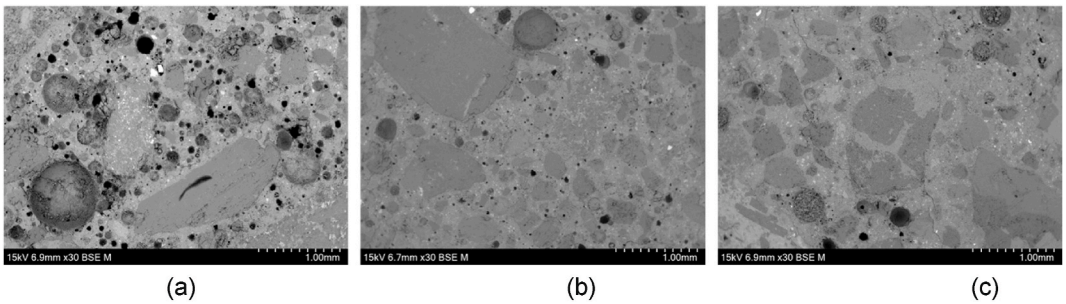

Fig. 6. SEM images (a) Control concrete, (b) 0.5 % CO_2 dosage and (c) 1 % CO_2 dosage.

Table 5
Analysis of air voids in SEM images using ImageJ.

Specimen	Count	Area (mm^2)	% Area	Mean
Control	274	0.238	1.81	255
0.5 % CO_2	72	0.062	0.46	255
1 % CO_2	24	0.048	0.35	255

Table 6
Statistical analysis of permeability coefficients, RCPT charge passed and concrete resistivity.

Mix (CO_2 dosage)	k (m/s)	RCPT (Coulombs)	Resistivity (kΩ-cm)
Control	1.41×10^{-11}	1989	15.71
0.25 %	7.06×10^{-12}	1447	17.27
0.50 %	1.85×10^{-12}	1407	19.09
0.75 %	9.46×10^{-13}	1222	19.09
1.00 %	1.68×10^{-12}	1146	17.26
Pearson correlation coefficient	k and RCPT	RCPT and Resistivity	k and Resistivity
	0.95	−0.69	−0.86
	Very strong positive linear relationship	Moderate negative linear relationship	Strong negative linear relationship

3.2. Freeze-thaw test

3.2.1. Mass loss

The mass loss was tested using the test procedure explained in ASTM C666-15, which is graphically represented in Fig. 7(a). The control concrete specimens indicated a larger mass loss of up to 0.25 %, as compared to other specimens with CO_2 addition, suggesting lower resistance under F-T conditions. The test results show that 0.75 % CO_2 dosage indicated the least mass loss, and it appears that the resistance of concrete to surface scaling and cracking under F-T conditions seems to improve with the addition of CO_2 during the mixing process.

3.2.2. Concrete resistivity

Fig. 7(b) graphically displays the surface resistivity of concrete measured using a Wenner probe. The concrete specimens with 0 % and 0.25 % CO_2 dosages indicated a lower resistivity of 18–20 kΩ-cm, which decreased with time, suggesting a higher permeability as compared to other dosages. The 0.5 % and 0.75 % CO_2 dosage mix shows a higher resistivity of 24–25 kΩ-cm at the start of the test and uniformly declines to 19.8 kΩ-cm after 300 cycles. The mix containing 1 % of the CO_2 showed the highest initial resistivity of 26.3 kΩ-cm and ended at 18.95 kΩ-cm after 300 cycles, suggesting lower permeability in comparison with other dosages. From the test results, it appears that a CO_2 dose of between 0.50 % and 0.75 % may provide optimum resistance to freeze-thaw resistance based on the resistivity test.

3.2.3. Young's modulus of elasticity and dynamic modulus of rigidity

Fig. 8(a) and (b) show Young's modulus of elasticity calculated from the fundamental transverse and longitudinal frequency for control concrete and mixes with varying CO_2 dosages. Additionally, the dynamic modulus of rigidity, calculated from fundamental torsional frequency, is illustrated in Fig. 9(a). The test results of the mix with 0.25 % CO_2 dose indicate the lowest elastic modulus and modulus of rigidity. The mix with 0.50 % CO_2 dosage shows the highest stiffness, with values between 56 and 57 GPa for transverse

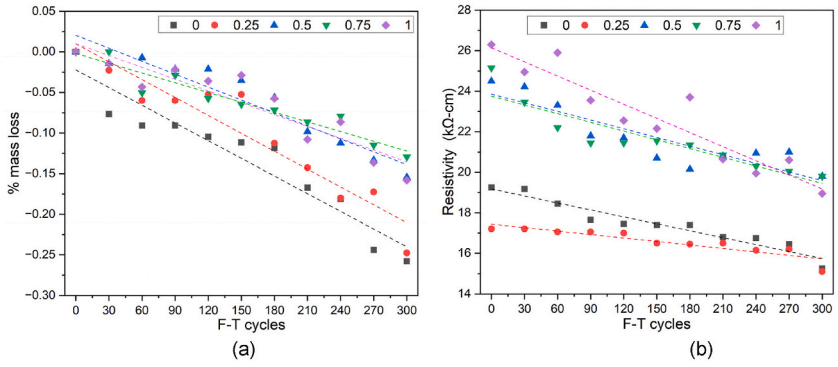

Fig. 7. (a) Percent mass loss and (b) Concrete Resistivity (kΩ-cm) at various F-T cycles.

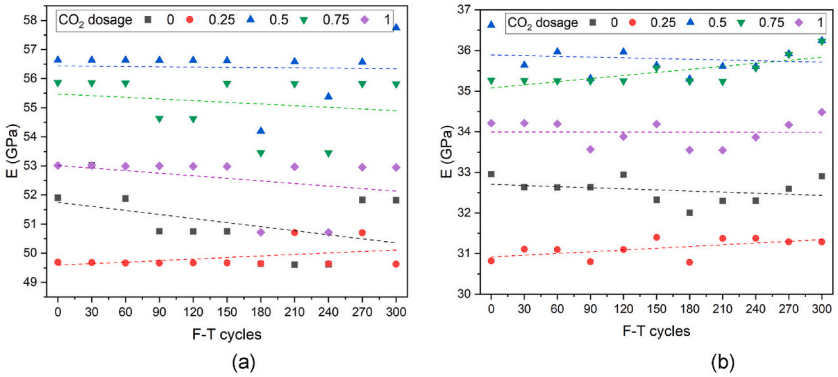

Fig. 8. Young's modulus of elasticity E (GPa) from (a) fundamental transverse frequency and (b) fundamental longitudinal frequency.

frequency, 36–37 GPa for longitudinal frequency and 8.6–8.6 GPa for torsional frequency. The mix with 0.75 % indicates stiffness values close to 0.50 % CO_2 dose mixes in all three cases. Higher dosages at 1 % CO_2 show a reduction in stiffness, indicating a threshold for CO_2 addition. This test suggests a dosage between 0.5 % and 0.75 % CO_2 addition provides an optimum stiffness and rigidity to concrete when subjected to F-T cycles, over control concrete mixes.

3.2.4. Dynamic modulus of elasticity from UPV

The dynamic modulus of elasticity calculated from the UPV wave velocity from Equation (10) in 300 F-T cycles has been graphically displayed in Fig. 9(b). The control mix shows a minor decrease in dynamic modulus of around 42 GPa, as compared to the other dosages, with 0.25 % CO_2 dosage indicating the least stiffness. The dynamic modulus values of the mixes containing 0.50 %, 0.75 % and 1 % CO_2 dosage indicate an improvement over control, between 44 and 46 GPa, with an increase in the number of F-T cycles and progress of hydration.

All the above test results for the F-T test show that the dynamic modulus of elasticity, dynamic modulus of rigidity, and resistivity values generally increase with CO_2 dosage, except at the 0.25 % dosage level. The stiffness values were highest in the CO_2 dosage range of 0.50 %–0.75 %, with a marginal improvement with the increase in F-T cycles suggesting improved bonding between the concrete particles. However, 1 % CO_2 dosages did not show a proportional increase in stiffness; instead, a decrease in elastic properties was observed, as seen in the test results displayed graphically. Visual observations from the Dynamic Modulus, UPV, and resistivity test results on concrete subjected to 300 F-T cycles suggest that the optimal CO_2 dosage range lies between 0.50 % and 0.75 %.

The results of the F-T test demonstrated that concrete mixes with 0.5 % and 0.75 % CO_2 dosage showed enhanced performance compared to the control concrete mix, as evidenced by lower mass loss, higher resistivity values, and improved dynamic modulus and stiffness properties. Early-age carbonation enhanced the pore structure, thereby limiting moisture absorption and the amount of freezable water while striking a balance between improved densification and retention of necessary pore space and flexibility to lower the risk of F-T damage. This reduction and retention of micropores were evident from the SEM imaging, as observed in Fig. 6. Conversely, at higher dosages (e.g., 1 %), early-age carbonation led to excessive densification, resulting in higher internal crystal pressure when subjected to F-T cycles. This is evident in the higher mass loss and lower dynamic modulus in concrete samples with 1 % CO_2 dosage, as compared to those with 0.5 % and 0.75 % dosages. These results indicate a threshold range for CO_2 dosing during the mixing stage, beyond which the benefits of carbonation tend to diminish for concrete subjected to F-T cycles. The 0.5 % and 0.75 % dosages fall within this threshold, offering enhanced F-T resistance compared to control concrete specimens, as well as a higher CO_2

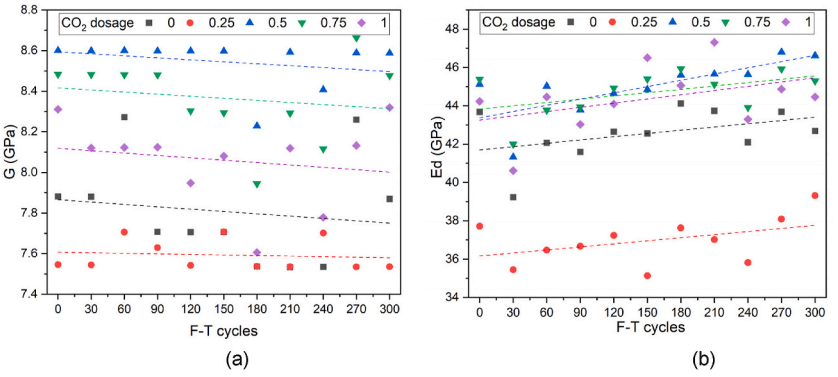

Fig. 9. (a) Dynamic modulus of rigidity from fundamental torsional frequency and (b) Dynamic modulus of elasticity from UPV.

dosage at 1 % and above.

3.3. Evaluation of pH of concrete

The pH of the powdered concrete samples extracted from specimens with CO_2 dosages ranging from 0.25 % to 1 %, including control concrete, at 90 days indicated a pH value between 12.05 and 12.16, as graphically represented in Fig. 10(b). Additionally, the phenolphthalein indicator test conducted on specimens at 90 days indicated a dark purple colour in all specimens, as shown in Fig. 11. These test results indicate that although the concrete samples were subjected to early-age carbonation, the alkalinity of the concrete remained sufficiently high, comparable to that of the control concrete. While the variation is small, it is important to note that early age carbonation at an optimal CO_2 dosage below 1 % by weight of cement in the mix ensures an alkaline environment inside concrete where the steel remains passivated.

3.4. Alternate wetting and drying cycles

3.4.1. Corrosion rate analysis

The average corrosion rate measured using the ICOR device for the concrete slab panels in sets A, C and B for different CO_2 dosages and environmental conditions at the 0^{th} and at the end of the 25th & 50th wetting and drying cycles are shown in Fig. 12(a), (b) & 12(c) respectively. The standard deviation of the average corrosion rate (average of 8 readings), measured by the ICOR device at each of the four nodes, in the horizontal and vertical positions for the respective slab panels are indicated as error bars on the bar graph. The authors of this paper acknowledge the high error observed in set B after 50 cycles, which may be due to a potential testing error caused by high corrosion of the embedded rebars.

In control concrete, as observed in all three sets, the initial corrosion rate was between 10 and 12 μm/year, measured after 28 days of curing immediately before starting the wetting and drying cycles. A study by Ali et al. [85] highlights that moisture in concrete and oxygen near the steel surface after 28 days of curing results in mild oxidation on the surface of the rebar. This activity takes place even in the highly alkaline environment of concrete, causing mild corrosion. The corrosion rate for the control concrete slab panel in set A drops at 25 cycles from 12.22 μm/year to 7.70 μm/year. However, by the 50th cycle, it increases marginally to 8.10 μm/year, suggesting that corrosion protection decreases with time due to environmental conditions. A rise in the corrosion rate was seen for the control concrete slab panel in set B throughout all cycles, especially between 25 and 50 cycles, when it increased from 56.40 μm/year to 105.40 μm/year. This suggests that the saline environmental conditions and a high temperature of 60 °C resulted in a high degree of corrosion. The control concrete slab panel in set C showed a moderate corrosion rate of 16.95 μm/year by the end of the 25th cycle and dropped to 5.97 μm/year by the end of the 50th cycle. The authors of this article hypothesize that this phenomenon may be attributed to the self-healing properties of concrete and ongoing hydration.

For the CO_2 sequestered concrete slab panels with 0.25 %, 0.5 % and 0.75 % CO_2 dosage, a decline in corrosion rate over time was observed for the slab panels in sets A and C, as compared to the control concrete slab panels, suggesting better performance with moderate CO_2 dosage and indicating the progress of hydration over time. For the 1 % CO_2 dosage, a reduction in corrosion rate over time was observed for set A. However, in the case of set C, the corrosion rate increased after 25 cycles from 10.98 μm/year to 14.92 μm/year and decreased by the 50th cycle to 4.42 μm/year. The authors of this article hypothesize that although corrosion protection mechanisms may initially be compromised due to environmental factors, self-healing properties and ongoing hydration in the concrete may help to mitigate some of the corrosion effects. Set B showed an increase in corrosion rate for all dosages from 0.25 % to 1 % CO_2

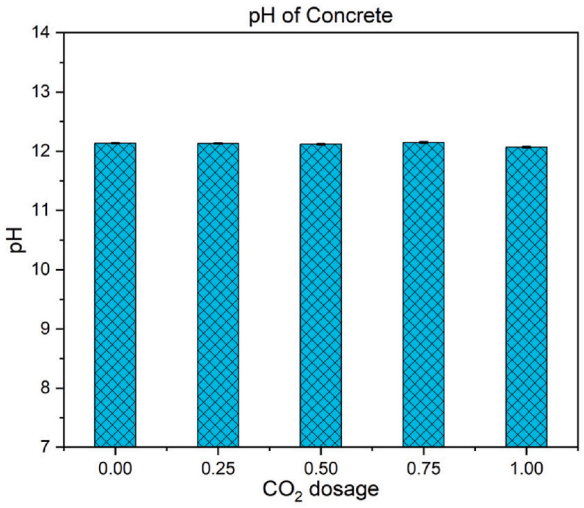

Fig. 10. pH of concrete.

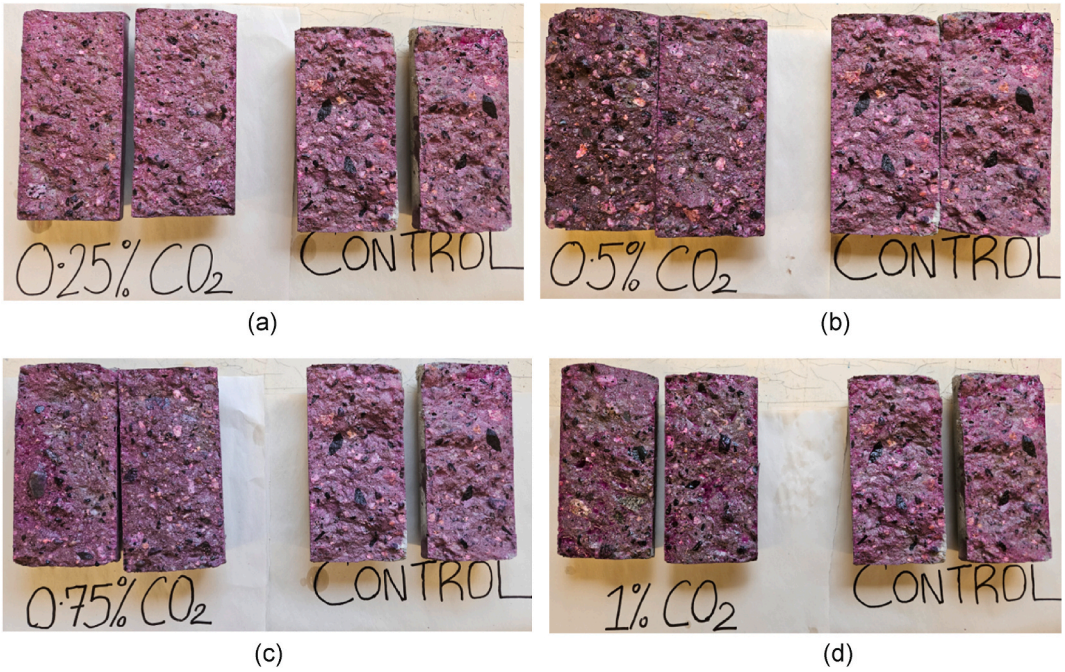

Fig. 11. Comparison of CO_2-sequestered concrete and control samples sprayed with phenolphthalein: (a) Control vs. 0.25 % CO_2, (b) Control vs. 0.5 % CO_2, (c) Control vs. 0.75 % CO_2, and (d) Control vs. 1.00 % CO_2.

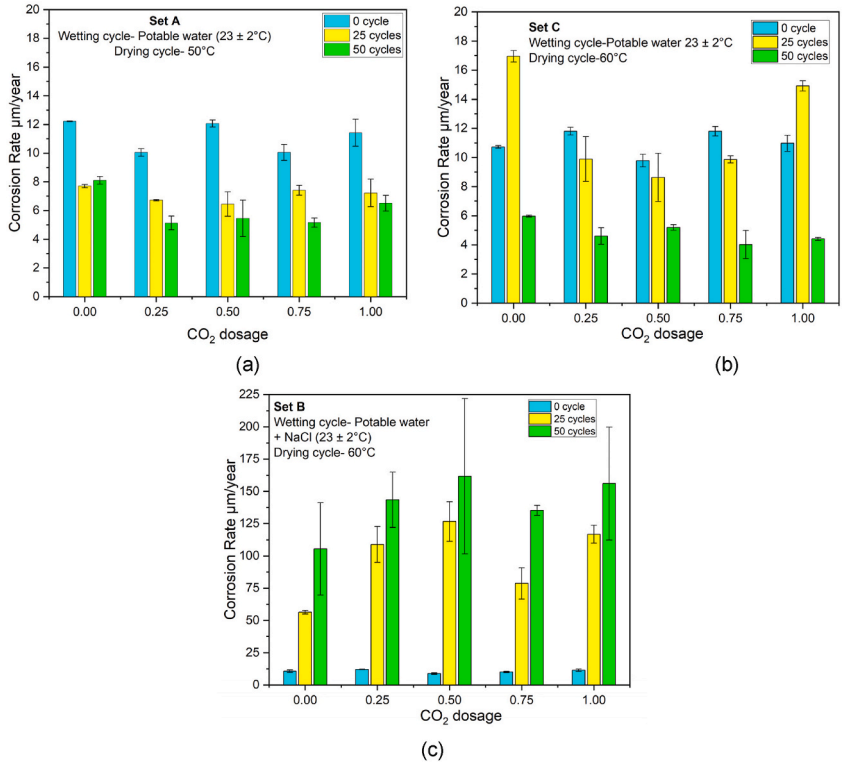

Fig. 12. Corrosion rate for concrete slab panels in (a) set A, (b) set C and (c) set B for different CO_2 dosages.

addition due to the high temperature of 60 °C during the drying cycle and immersion in water with a 5 % NaCl concentration during the wetting cycles, indicating chloride-induced corrosion. This suggests that adding CO_2 alone cannot enhance the durability of concrete under harsh and saline environmental conditions.

This corrosion analysis indicated that CO_2-sequestered concrete at dosages between 0.25 % and 0.75 % exhibited a reduction in corrosion rates over time when subjected to high temperatures but in chloride-free environments (Sets A and C). Control concrete samples in sets A and C experienced varying corrosion rates influenced by environmental factors. This trend indicates that early-age or accelerated carbonation, when optimized, can enhance the corrosion resistance of reinforced concrete, likely due to improved microstructural densification, which limits oxygen and moisture ingress to initiate corrosion of embedded rebars in concrete. Conversely, neither control nor CO_2-sequestered concrete could withstand the harsh saline conditions (Set B), which led to increased corrosion rates. This highlights the limitations of early age carbonation in enhancing the durability of concrete, over control, under harsh saline environmental exposures and thermal stresses. In order to withstand aggressive environmental conditions reinforced concrete would have to be designed with corrosion inhibitors and supplementary cementitious materials and adopt good concrete practices to avoid cracks and prevent the entry of water and degrading salts into the body of concrete.

3.4.2. Concrete resistivity analysis

The average resistivity measured by the ICOR device and the Wenner probe for the concrete slab panels in sets A, C and B for different CO_2 dosages are illustrated in Fig. 13(a), (b) & 13(c) the 0^{th}, and at the end of the 25th & 50th wetting and drying cycles. The standard deviation of the average resistivity readings for the respective slab panels are indicated as error bars on the bar graph. The average resistivity is calculated using eight measurements taken by the ICOR device at four nodes (in both horizontal and vertical positions) and four measurements obtained using the Wenner probe in the four quadrants of the respective slab panels. Resistivity measured by both devices indicates that control and CO_2-sequestered concrete show an improvement in resistivity as hydration progresses. For the 0.5 % CO_2 dosage, there has been an improvement in resistivity values from 11.78 kΩ-cm to 26.69 kΩ-cm in set A and from 7.88 kΩ-cm and 25.38 kΩ-cm in set C. These values are higher compared to other dosages, indicating that CO_2 dosing at a particular threshold improves the resistivity of concrete and thereby enhances its long-term durability. The electrical resistivity for all the slab panels in set B decreased for all dosages, including control concrete. This suggests that adding CO_2 alone to concrete is insufficient to resist the risk of chloride-induced corrosion when exposed to extreme weather conditions and corrosive salts.

3.4.3. Half-cell potential analysis

The half-cell potential or voltages measured using a copper-copper sulphate half-cell and a digital multimeter for the concrete slab panels in sets A and C for different CO_2 dosages are illustrated in Fig. 14(a) and (b), respectively. These values are measured at the 0^{th}

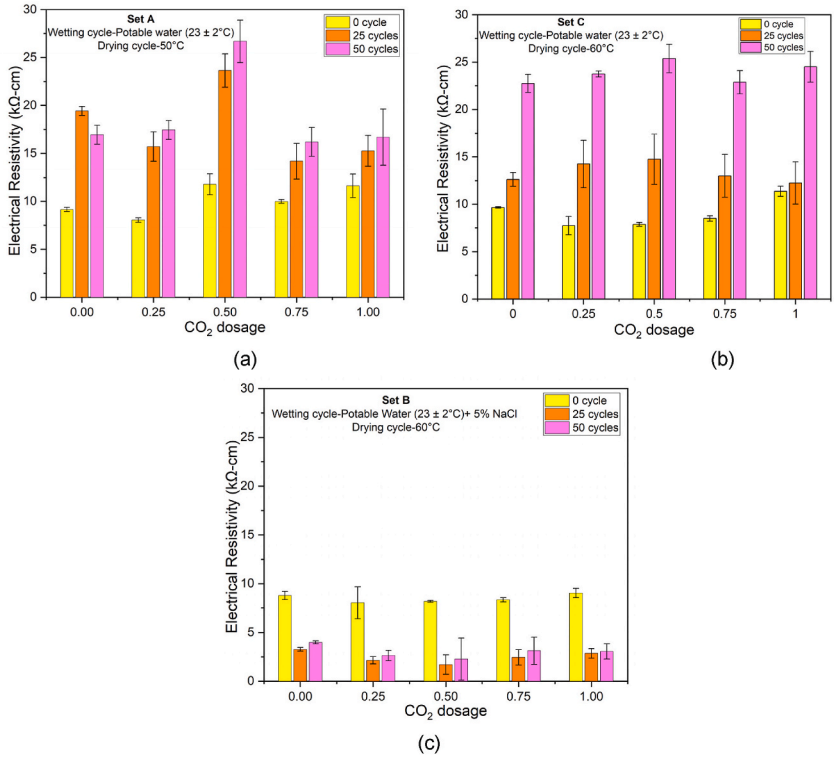

Fig. 13. Concrete resistivity for concrete slab panels in (a) set A,(b) set C and (c) set B for different CO_2 dosages.

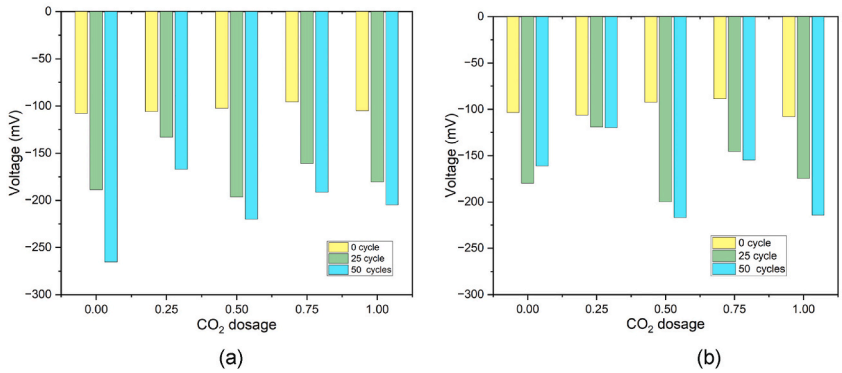

Fig. 14. (a) Half-cell potential for concrete slab panels in (a) set A and (b) set C for different CO_2 dosages.

Table 7
Half Cell Potential criteria according to ASTM C876-15.

Half-cell potential (mV)	Probability of corrosion
>−200	Less than 10 %
−200 to −350	Uncertain
<−350	More than 90 %

cycle and at the end of the 25th & 50th wetting and drying cycles. The concrete slab panels in set B did not show any potential difference or voltage readings on the multimeter at the end of the 25th and 50th cycles, indicating severe corrosion for all CO_2 dosages, including control concrete. This may have been due to the formation of rust, which is generally non-conductive and creates a discontinuity in the electrical contact with the rebar. The voltage readings at the 0 cycle were in line with the readings for samples A and C; however, as there were no readings on the multimeter for the 25th and 50th cycle, the data of the 0^{th} cycle for sample B has not been plotted. As per the criteria provided in ASTM C876-15 [83] for a Cu-$CuSO_4$ electrode, which has been detailed in Table 7, the probability of corrosion up to 10 % was observed in all concrete slab panels. The concrete slab panels with 0.25 % CO_2 dosage, in both sets A and C, indicate a lower probability of corrosion as compared to other CO_2 dosages. This test also indicates that mineralization, through CO_2 alone, cannot provide resistance to corrosion under harsh environmental conditions.

The alternative wetting and drying cycles test demonstrates improved corrosion rate, resistivity and half-cell potential for concrete slab panels in sets A and C for dosages between 0.5 % and 0.75 % as compared to control concrete, which were subjected to high temperatures without chloride salt exposure. However, the harsh environmental conditions of high temperature and salt solution (5 % NaCl) for concrete slab panels in set B potentially led to corrosion for all CO_2 dosages including control concrete, as indicated by the test data. The authors of this paper feel that when concrete is exposed to chloride salts and high temperatures, CO_2 sequestration alone cannot provide corrosion resistance, and supplementary techniques will have to be adopted.

4. Predicting the service life of reinforced concrete subjected to accelerated corrosion

Literature has documented well-established corrosion models that can be used to understand the behaviour of reinforced concrete under different environmental conditions. As part of this study, the authors have adopted the Tuutti model to estimate the service life of reinforced concrete subjected to accelerated corrosion. As explained by Tuutti [78], this model divides the corrosion process into two main phases: the Initiation phase and the Propagation phase. The initiation phase is the time taken for chlorides to penetrate the concrete cover and reach the rebar at a critical concentration. Tuutti explains that the steel reinforcement becomes de-passivated during this time due to the deterioration of the passive protective oxide coating. The author also describes how corrosion begins during the propagation phase, causing damage to the concrete and possibly structural failure. The service life model, as described by Tuutti, has been shown in equation (9), and the progress of the corrosion of steel in concrete has been schematically illustrated in Fig. 15. Based on the test results from RCPT, corrosion rate and resistivity data under the two exposure conditions for alternative wetting and drying conditions, for the five CO_2 dosages varying from 0 % to 1 %, the Tuutti model has been referred to estimate the service life of concrete. This analysis aims to compare the corrosion resistance of CO_2-sequestered concrete over control and check if early-age carbonation helps to enhance the service life of reinforced concrete structures.

$$T_{service} = T_{initial} + T_{propagation} \quad (9)$$

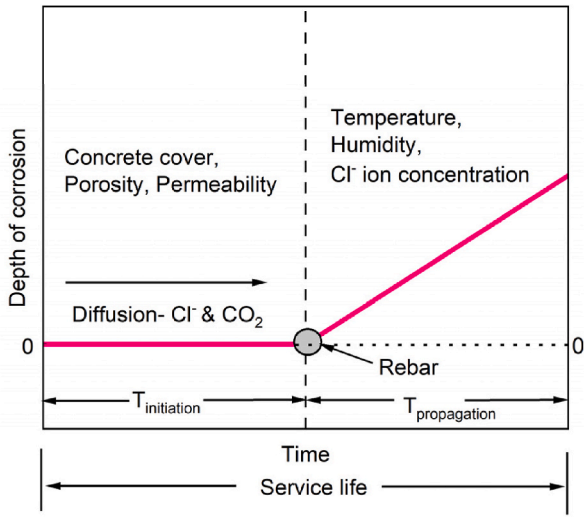

Fig. 15. Schematic sketch of steel corrosion in concrete (Tuutti 1982) [78].

4.1. Initiation time ($T_{initiation}$)

As explained by Tuutti [78], the initiation time indicates the period during which the chloride ions from the concrete surface penetrate the clear concrete cover to reach the rebars and to start the onset of corrosion. The factors affecting the initiation time include the porosity and permeability of concrete, the chloride ion diffusion coefficient, the clear concrete cover, the critical chloride threshold and the surface ion concentration, which mainly depends upon the environmental conditions. As described by Justnes et al. [86], equation (10) illustrates how Fick's Second Law of Diffusion is typically used to determine the onset time for chloride ion penetration.

$$\frac{\Delta C}{\Delta t} = D\frac{\Delta^2 C}{\Delta x^2} \tag{10}$$

Where, $\frac{\Delta C}{\Delta t}$ represents the rate of change of concentration (C) with respect to time (t). $\frac{\Delta^2 C}{\Delta x^2}$ represents the second spatial derivative of concentration (C) with respect to the spatial position from the surface (x), indicating the rate of change of concentration over distance.

In order to determine the initiation time in this study, equation (11) has referred to the article by Dinh [87], who used Fick's second law of diffusion to obtain the concentration at a specific depth from the surface.

$$\mathrm{Ct} = \mathrm{Cs}\left[1 - \mathrm{erf}\left(\frac{x}{2\sqrt{Dt}}\right)\right] \tag{11}$$

Where, Ct is the concentration as a depth x from the surface at time t, Cs is the surface concentration, x is the depth within concrete, and D is the diffusion coefficient for concrete.

To determine the initiation time ($T_{initiation}$ in seconds), Justnes et al. [86] have modified equation (11) in terms of the clear concrete cover, diffusion coefficient (D, in m^2/sec) and the error function, as shown in equation (12).

$$\mathrm{Tinitiation} = \frac{x^2}{4D}\,\frac{1}{\left[\mathrm{erf}^{-1}\left(1 - \left(\frac{\mathrm{Ct}}{\mathrm{Cs}}\right)\right)\right]^2} \tag{12}$$

Where x is the clear cover depth (m), which is 30 mm for this test, Ct is the critical chloride threshold, and Cs is the surface ion concentration. The value of Ct/Cs has been taken as 0.6, as provided in ACI 365.1R00, assuming Ct to be 0.4 % by mass of cement [88].

The diffusion coefficient has been determined using the Nernst-Einstein equation, as described by Konecny et al. [89] as shown in equation (13).

$$\mathrm{D} = \frac{\mathrm{R\ T\ t}_i}{\mathrm{Z}^2\ \mathrm{F}^2\ \gamma_i\ Ci\ \rho_{BR}} \tag{13}$$

Where R universal gas constant (8.31446 J/mol.K), T absolute temperature (296.15°K- as the test is conducted at 23 °C), and the Faraday's constant (F) is 96500 C/mol. The Z valence of ions [−], the transport number (t_i) of chloride ions [−] and γ_i activity coefficient of chloride ions [−] is assumed to be 1, as described by Konecny et al. Ci represents the molar weight of the solution in mol/m^3. The molar concentration of chloride ions for a 3 % NaCl solution, with the molar weight of NaCl being 58.44 g/mol, is 513.3 mol/m^3.

The volumetric electrical resistivity ρ_{BR} (Ω-m) which is described by Konecny et al. and obtained from the RCPT in equation (14).

$$\rho_{BR} = \frac{VtA}{QL} \tag{14}$$

Where V represents the electrical potential applied during the test (60 V), t is the test duration (6 h or 21,600 s), A is the cross-sectional area of the specimen (m^2) for a sample with a 100 mm diameter, Q is the total electrical charge in coulombs that passed through the specimen, and L is the sample thickness, which was 50 mm. These parameters comply with the requirements outlined in ASTM C1202-22.

4.2. Propagation time ($T_{propogation}$)

As explained by Tuutti [78], the propagation time indicates the period between the initiation of corrosion of rebars in concrete and until complete degradation takes place. The author further explains that the time to corrosion propagation depends on the critical steel loss ($d_{critical}$ in μm) and corrosion rate (ν_{corr} in μm /year), as summarized in equation (15). The corrosion rate for this study was obtained directly from the ICOR device, and it can also be derived from Faraday's law if the corrosion current is known. Broomfield [17] highlights that cracking is induced by less than 100 μm of steel section loss for structural deterioration to begin. For the calculation of propagation time, $d_{critical}$ has been assumed to be 100 μm.

$$T_{propogation} = \frac{d_{critical}}{\nu_{corr}} \tag{15}$$

4.3. Service life prediction

Tuutti's model has been used in this study to determine the service life of the structure by combining the corrosion initiation and progression time relationships. Table 8 provides an analysis of the estimated service life of concrete mixes with different CO_2 dosages during mixing. The parameters include RCPT values, resistivity (ρBR), diffusion coefficient, initiation time, corrosion rate, and propagation time, which have been used to estimate the overall service life. The accelerated corrosion test, by subjecting the reinforced concrete slabs to alternative wetting and drying cycles, has been used to speed up the natural corrosion process. The authors of this paper believe that service life estimations in Table 8 might be conservative, as the data is based on accelerated tests. However, the intention is to use these estimations for comparing CO_2-sequestered concrete with control concrete. Additionally, Broomfield [17] explains that the propagation period in actual structures is expected to be longer than the propagation time observed in accelerated tests, assuming the structure is in a moderate or controlled environment.

Table 8 shows that the control mix has the shortest service life. The high RCPT, low resistivity and high corrosion rate of control concrete, compared to the mixes with CO_2 addition, led to a shorter initiation and propagation phase and decreased overall service life. The 0.25 %, 0.50 % and 0.75 % CO_2 dosage provided improvements as compared to the control mix, with 0.75 % CO_2 dosage indicating the most extended service life. Although the 1.00 % CO_2 mix had the maximum resistance to chloride ingress, its higher corrosion rate as compared to 0.75 % reduced its service life to 36.3 years as compared to 38.6 years observed with 0.75 % CO_2 dosage, indicating a threshold of CO_2 benefits to corrosion resistance. This analysis demonstrates that a CO_2 dosage between 0.5 % and 0.75 % would provide optimum performance during the initiation and propagation phase.

Table 8
Assessment of the estimated service life of reinforced concrete.

Mix (CO_2 dosage)	RCPT (Coulombs)	ρ_{BR} (kΩ-cm)	Diffusion coefficientm/$s^{2[a]}10^{-12}$	$T_{initiation}$ (years)	Average ν_{corr} (μm /year)	Average $T_{propogation}$ (years)	[a]$T_{service}$ (years)
Control	1989	10.24	5.03	10.3	7.04	14.2	24.6
0.25 %	1447	14.07	3.66	14.2	4.87	20.5	34.8
0.50 %	1407	14.47	3.56	14.6	5.32	18.8	33.4
0.75 %	1222	16.66	3.09	16.8	4.59	21.8	38.6
1.00 %	1146	17.76	2.90	18.0	5.46	18.3	36.3

Note.
[a] calculated under accelerated conditions. Average ν_{corr} corresponds to the average corrosion rate of concrete slab panels in sets A & C at the end of 50 wetting and drying cycles.

5. Concluding remarks

This study investigated the long-term effects of early-age carbonation on the durability of CO_2-sequestered concrete by evaluating its transport properties, freeze-thaw resistance and corrosion behaviour under varying environmental conditions. The experimental approach adopted in this study focussed on resistivity, chloride ion penetration, water permeability, dynamic modulus under freeze-thaw cycles, corrosion rate and corrosion potential of reinforced concrete subjected to alternative wetting and drying conditions. The test results shed light on the benefits of early-age carbonation on the long-term durability of concrete in terms of lowered permeability and chloride ion penetration, enhanced resistivity, and improved freeze-thaw and corrosion resistance. The findings from this study reveal that CO_2 dosages between 0.5 % and 0.75 % provided optimal results in terms of resistivity, stiffness and corrosion resistance compared to control concrete. However, the test results also revealed a threshold in CO_2 addition at 1 %, as observed in reducing these parameters.

5.1. Conclusions

1. The test result indicates an overall improvement in the durability of CO_2 sequestered concrete, which has been observed with lower RCPT and permeability values and higher resistivity readings between 0.5 % and 1 % dosage.
2. CO_2 dosages between 0.5 % and 0.75 % showed improved performance to F-T cycles, as compared to control concrete, observed by lower mass loss and surface scaling and increased stiffness. Higher dosages can reduce the F-T resistance due to the densification effect.
3. Even though the concrete was subjected to accelerated carbonation, the alkalinity of the concrete was sufficiently high to resist the onset of corrosion, as observed by the pH of the concrete.
4. Reinforced concrete panels with 0.5 %–0.75 % CO_2 dosage showed improved corrosion resistance under high temperatures in salt-free environments. However, all panels, including the control, experienced increased corrosion rates in saline conditions. This highlights the need for adding supplementary cementitious materials and rebar coatings, in addition to CO_2 sequestration, to enhance durability in aggressive environments.
5. Predicting the service life by applying Tuutti's model to the experimental results indicates that a CO_2 dosage between 0.5 % and 0.75 % provides an enhanced service life of reinforced concrete.

These conclusions reinforce the hypothesis that concrete specimens subjected to early-age carbonation will maintain the alkalinity of concrete, decrease permeability and chloride ion ingress, enhance resistance to F-T cycles and protect embedded rebars from corrosion. The improvement in concrete properties observed is limited to the specific concrete mixes evaluated in this study. The authors suggest that further research should be conducted across a broader range of concrete mix designs with different cement and cementitious materials under varying environmental conditions. Additionally, the issue of loss of workability of concrete after CO_2 addition also needs to be addressed.

This research contributes to the body of knowledge on the long-term impact of CO_2 sequestration on concrete performance and durability. As natural carbonation has had sufficient evidence to prove corrosion of rebars and deterioration to surrounding concrete, there are apprehensions within the engineering community to adopt CO_2 sequestering in concrete during the mixing stage. The results from this study would provide valuable insights for decision-makers to explore the implementation of CO_2 sequestering in concrete in the ready-mix concrete industry across the globe.

5.2. Limitations of this study

- This study used commercially available pure CO_2 gas, as effluent CO_2 captured through carbon capture technologies was not readily available. The effect of CO_2 captured from industrial emissions on the properties of concrete in plastic and hardened stages could not be determined.
- The durability performance was evaluated under accelerated conditions, and long-term performance data for CO_2-sequestered concrete under natural exposure conditions is not unavailable.
- The study focused on a maximum CO_2 dosage of 1 % by weight of cement, as increasing the dosage had an adverse impact on the workability of the concrete mix. The impact of higher dosages of durability has not been studied.
- The effects of different cement types and supplementary cementitious materials were not explored in this study.

5.3. Recommendations for future work

- Experimental research on the use of CO_2 sourced from carbon capture technologies is required to assess the impact of industrial-grade effluent gases on fresh and hardened properties of concrete.
- Effect of CO_2-sequestration on the durability of concrete under natural environmental exposures over extended periods is required to validate the findings from the accelerated tests.
- Studies should focus on improving the workability of concrete at higher CO_2 dosages, and further exploration is needed to assess its impact on durability.
- The effect of different cement types and supplementary cementitious materials, along with their compatibility with CO_2 sequestration, should be studied to understand their impact on concrete performance in fresh and hardened stages.

- A life cycle assessment needs to be done to assess the environmental impacts of CO_2-sequestered concrete across all stages of its life cycle, including raw material extraction, production, usage, and end-of-life.

In a nutshell, the authors feel that sequestering CO_2 in concrete would help the concrete industry develop a green and sustainable building material.

CRediT authorship contribution statement

Clinton Pereira: Writing – original draft, Visualization, Validation, Software, Methodology, Investigation, Data curation. **Rishi Gupta:** Writing – review & editing, Supervision, Resources, Project administration, Funding acquisition, Conceptualization.

Informed consent statement

Not applicable.

Data availability statement

Some or all data that support the findings of this study are available from the corresponding author upon reasonable request.

Institutional review board statement

Not applicable.

Declaration of generative AI in scientific writing

Not applicable.

Funding

This research received financial support from Dr.Rishi Gupta's NSERC-Discovery grant, Canada.

Declaration of competing interest

The authors declare the following financial interests/personal relationships which may be considered as potential competing interests:This research received financial support from Dr.Rishi Gupta's NSERC-Discovery grant, Canada. If there are other authors, they declare that they have no known competing financial interests or personal relationships that could have appeared to influence the work reported in this paper.

Acknowledgements

The authors extend their sincere gratitude to FIMIM and CAMTEC for providing their experimental facilities. The dedicated efforts of co-op students, Hannah Bochmann and Ailish Paterson, in assisting with all the experimental work is sincerely acknowledged and truly appreciated. We sincerely thank Dr. Armando Tura, Arielle Garrett, Bastien Lanusse and Solomon Rosenberg from the tech support team at UVic for their invaluable assistance. We thank Drs. Cristina Cordoba and Elaine Humphrey from the Advanced Microscopy facility at CAMTEC for helping us with the SEM analysis. We are grateful to our colleagues Jay Viradiya, Dr. Loveleen Sharma, Prakriti Raizada, Navid Tutkaboni, for their support on this project. Finally, we thank Aarti Pereira for proofreading the final version of this paper.

Data availability

Data will be made available on request.

References

[1] Industrial revolution and technology. https://education.nationalgeographic.org/resource/industrial-revolution-and-technology. (Accessed 13 February 2025).
[2] K. Ahmed Ali, M. Ahmad, Y. Yusup, Issues, impacts, and mitigations of carbon dioxide emissions in the building sector, Sustainability 12 (Sep. 2020) 7427, https://doi.org/10.3390/su12187427.
[3] B. Dziejarski, R. Krzyżyńska, K. Andersson, Current status of carbon capture, utilization, and storage technologies in the global economy: a survey of technical assessment, Fuel 342 (Jun. 2023) 127776, https://doi.org/10.1016/j.fuel.2023.127776.
[4] Global cement and concrete industry announces roadmap to achieve groundbreaking 'net zero' co2 emissions by 2050, GCCA, https://gccassociation.org/news/global-cement-and-concrete-industry-announces-roadmap-to-achieve-groundbreaking-net-zero-co2-emissions-by-2050/. (Accessed 19 December 2023).
[5] M. Auroy, et al., Comparison between natural and accelerated carbonation (3% CO2): impact on mineralogy, microstructure, water retention and cracking, Cement Concr. Res. 109 (Jul. 2018) 64–80, https://doi.org/10.1016/j.cemconres.2018.04.012.

[6] M. Fernández Bertos, S.J.R. Simons, C.D. Hills, P.J. Carey, A review of accelerated carbonation technology in the treatment of cement-based materials and sequestration of CO2, J. Hazard Mater. 112 (3) (Aug. 2004) 193–205, https://doi.org/10.1016/j.jhazmat.2004.04.019.
[7] N.L.M. Kamal, Z. Itam, Y. Sivaganese, S. Beddu, Carbon dioxide sequestration in concrete and its effects on concrete compressive strength, Mater. Today Proc. 31 (Jan. 2020) A18–A21, https://doi.org/10.1016/j.matpr.2020.11.185.
[8] J. Zhu, S. Liu, L. Song, Z. Qu, H. Wang, Influence of carbon dioxide curing on the corrosion resistance of reinforced cement mortar under the external erosion of NaCl freeze–thaw cycle, Appl. Sci. 12 (10) (Jan. 2022) 10, https://doi.org/10.3390/app12105061.
[9] A.F.A. Fuhaid, A. Niaz, Carbonation and corrosion problems in reinforced concrete structures, Buildings 12 (5) (May 2022) 5, https://doi.org/10.3390/buildings12050586.
[10] S. Mindess, J.F. Young, D. Darwin, Concrete, in: Prentice-hall Civil Engineering and Engineering Mechanics Series, Prentice Hall, 2003. https://books.google.ca/books?id=euMXnwEACAAJ.
[11] B. Šavija, M. Luković, Carbonation of cement paste: understanding, challenges, and opportunities, Constr. Build. Mater. 117 (Aug. 2016) 285–301, https://doi.org/10.1016/j.conbuildmat.2016.04.138.
[12] W. Ashraf, Carbonation of cement-based materials: challenges and opportunities, Constr. Build. Mater. 120 (Sep. 2016) 558–570, https://doi.org/10.1016/j.conbuildmat.2016.05.080.
[13] A. Leemann, F. Moro, Carbonation of concrete: the role of CO2 concentration, relative humidity and CO2 buffer capacity, Materials and Structures/Materiaux et Constructions 50 (1) (2017), https://doi.org/10.1617/s11527-016-0917-2.
[14] R.A. Robayo-Salazar, A.M. Aguirre-Guerrero, R. Mejía de Gutiérrez, Carbonation-induced corrosion of alkali-activated binary concrete based on natural volcanic pozzolan, Constr. Build. Mater. 232 (Jan. 2020) 117189, https://doi.org/10.1016/j.conbuildmat.2019.117189.
[15] A. Marani, T. Oyinkanola, D.K. Panesar, Probabilistic deep learning prediction of natural carbonation of low-carbon concrete incorporating SCMs, Cement Concr. Compos. 152 (Sep. 2024) 105635, https://doi.org/10.1016/j.cemconcomp.2024.105635.
[16] U.M. Angst, Steel corrosion in concrete – Achilles' heel for sustainable concrete? Cement Concr. Res. 172 (Oct. 2023) 107239 https://doi.org/10.1016/j.cemconres.2023.107239.
[17] J. Broomfield, Corrosion of Steel in Concrete: Understanding, Investigation and Repair (2022), https://doi.org/10.1201/9781003223016.
[18] M. Basheer, D.P. Russell, G.I.B. Rankin, "Design of concrete to resist carbonation, in: 8th International Conference on Durability of Building Materials and Components (8dbmc), May 1999, pp. 423–435.
[19] V. Rostami, Y. Shao, A.J. Boyd, Durability of concrete pipes subjected to combined steam and carbonation curing, Constr. Build. Mater. 25 (8) (Aug. 2011) 3345–3355, https://doi.org/10.1016/j.conbuildmat.2011.03.025.
[20] B. Lagerblad, Carbon Dioxide Uptake during Concrete Life Cycle - State of the Art, Swedish Cement and Concrete Research Institute, Jan. 2005.
[21] Y. Shao, Beneficial Use of Carbon Dioxide in Precast Concrete Production, Jun. 2014 1155035, https://doi.org/10.2172/1155035.
[22] S. Monkman, M. MacDonald, R.D. Hooton, P. Sandberg, Properties and durability of concrete produced using CO2 as an accelerating admixture, Cement Concr. Compos. 74 (Nov. 2016) 218–224, https://doi.org/10.1016/j.cemconcomp.2016.10.007.
[23] P. Claisse, Transport Properties of Concrete: Measurements and Applications, 2014.
[24] Y. Li, Z. Liu, J. Jiang, Microstructure and macroscopic properties of low-carbon concrete subjected to elevated temperature: state-of-the-Art Review, J. Build. Eng. 86 (Jun. 2024) 108731, https://doi.org/10.1016/j.jobe.2024.108731.
[25] P. Azarsa, R. Gupta, Electrical resistivity of concrete for durability evaluation: a review, Adv. Mater. Sci. Eng. 2017 (1) (2017) 8453095, https://doi.org/10.1155/2017/8453095.
[26] X. Li, Q. Xu, S. Chen, An experimental and numerical study on water permeability of concrete, Constr. Build. Mater. 105 (Feb. 2016) 503–510, https://doi.org/10.1016/j.conbuildmat.2015.12.184.
[27] E.J. Garboczi, Permeability, diffusivity, and microstructural parameters: a critical review, Cement Concr. Res. 20 (4) (Jul. 1990) 591–601, https://doi.org/10.1016/0008-8846(90)90101-3.
[28] K. Li, F. Zhao, Y. Zhang, 胡振中, Influence of carbonation on the chloride ingress into concrete: theoretical analysis and application to durability design, Cement Concr. Res. 123 (Jun. 2019), https://doi.org/10.1016/j.cemconres.2019.105788.
[29] G.A. Julio-Betancourt, R.D. Hooton, Study of the Joule effect on rapid chloride permeability values and evaluation of related electrical properties of concretes, Cement Concr. Res. 34 (6) (Jun. 2004) 1007–1015, https://doi.org/10.1016/j.cemconres.2003.11.012.
[30] R. Feldman, L.R. Prudencio, G. Chan, Rapid chloride permeability test on blended cement and other concretes: correlations between charge, initial current and conductivity, Constr. Build. Mater. 13 (3) (Apr. 1999) 149–154, https://doi.org/10.1016/S0950-0618(98)00033-6.
[31] R. Spragg, et al., Leaching of conductive species: implications to measurements of electrical resistivity, Cement Concr. Compos. 79 (May 2017) 94–105, https://doi.org/10.1016/j.cemconcomp.2017.02.003.
[32] A.A. Ramezanianpour, A. Pilvar, M. Mahdikhani, F. Moodi, Practical evaluation of relationship between concrete resistivity, water penetration, rapid chloride penetration and compressive strength, Constr. Build. Mater. 25 (5) (May 2011) 2472–2479, https://doi.org/10.1016/j.conbuildmat.2010.11.069.
[33] S. Gupta, Carbon sequestration in cementitious matrix containing pyrogenic carbon from waste biomass: a comparison of external and internal carbonation approach, J. Build. Eng. 43 (Nov. 2021) 102910, https://doi.org/10.1016/j.jobe.2021.102910.
[34] N. Kamal, Z. Itam, Y. Sivaganese, S. Beddu, Carbon dioxide sequestration in concrete and its effects on concrete compressive strength, Mater. Today Proc. 31 (Dec. 2020), https://doi.org/10.1016/j.matpr.2020.11.185.
[35] I. Elkhaldi, E. Rozière, G. Villain, A. Loukili, Effect of accelerated carbonation on electrical resistivity and microstructure of clinker-slag-limestone cement based concretes, Mater. Struct. 57 (Jan) (2024), https://doi.org/10.1617/s11527-023-02290-x.
[36] D. Singh Gill, S. Mariam Abraham, Feasibility of CO2 sequestration in concrete containing recycled aggregates, Mater. Today Proc. (Mar. 2023), https://doi.org/10.1016/j.matpr.2023.03.186.
[37] Y. Zhao, S. Lian, J. Bi, C. Wang, kun Zheng, Study on Freezing-Thawing damage mechanism and evolution model of concrete, Theor. Appl. Fract. Mech. 121 (Oct. 2022) 103439, https://doi.org/10.1016/j.tafmec.2022.103439.
[38] H. Cai, X. Liu, Freeze-thaw durability of concrete: ice formation process in pores, Cement Concr. Res. 28 (9) (Sep. 1998) 1281–1287, https://doi.org/10.1016/S0008-8846(98)00103-3.
[39] ACI 201.2R-16 guide to durable concrete. https://www.concrete.org/publications/internationalconcreteabstractsportal/m/details/id/51689514. (Accessed 25 July 2024).
[40] S. Fajardo, D.M. Bastidas, M.P. Ryan, M. Criado, D.S. McPhail, J.M. Bastidas, Low-nickel stainless steel passive film in simulated concrete pore solution: a SIMS study, Appl. Surf. Sci. 256 (21) (Aug. 2010) 6139–6143, https://doi.org/10.1016/j.apsusc.2010.03.140.
[41] F. Shaheen, B. Pradhan, Influence of sulfate ion and associated cation type on steel reinforcement corrosion in concrete powder aqueous solution in the presence of chloride ions, Cement Concr. Res. 91 (Jan. 2017) 73–86, https://doi.org/10.1016/j.cemconres.2016.10.008.
[42] N. Silva, Chloride induced corrosion of reinforcement steel in concrete - threshold values and ion distributions at the concrete-steel interface. https://www.semanticscholar.org/paper/Chloride-Induced-Corrosion-of-Reinforcement-Steel-Silva/42906505c6370ea601f0e2946e17545fec08fb36, 2013. (Accessed 25 August 2024).
[43] B. Guo, G. Chu, R. Yu, Y. Wang, Q. Yu, D. Niu, Effects of sufficient carbonation on the strength and microstructure of CO2-cured concrete, J. Build. Eng. 76 (Oct. 2023) 107311, https://doi.org/10.1016/j.jobe.2023.107311.
[44] A. Steffens, D. Dinkler, H. Ahrens, Modeling carbonation for corrosion risk prediction of concrete structures, Cement Concr. Res. 32 (6) (Jun. 2002) 935–941, https://doi.org/10.1016/S0008-8846(02)00728-7.
[45] S. Talukdar, N. Banthia, Carbonation in concrete infrastructure in the context of global climate change: development of a service lifespan model, Constr. Build. Mater. 40 (Mar. 2013) 775–782, https://doi.org/10.1016/j.conbuildmat.2012.11.026.
[46] X. Shen, et al., Combine ingress of chloride and carbonation in marine-exposed concrete under unsaturated environment: a numerical study, Ocean Eng. 189 (Oct. 2019) 106350, https://doi.org/10.1016/j.oceaneng.2019.106350.

[47] CAN/CSA-A3000-03. Cementitious materials compendium (Consists of A3001, A3002, A3003, A3004 and A3005), CSA Group, https://www.csagroup.org/store/product/2416710/. (Accessed 25 August 2024).
[48] ASTM International, ASTM C595-08a standard specification for blended hydraulic cements. https://www.astm.org/c0595-08a.html. (Accessed 26 August 2023).
[49] ASTM International, ASTM C33/C33M-18 standard specification for concrete aggregates. https://www.astm.org/c0033_c0033m-18.html. (Accessed 26 August 2023).
[50] ASTM International, C494/C494M-17 standard specification for chemical admixtures for concrete. https://www.astm.org/c0494_c0494m-17.html. (Accessed 26 August 2023).
[51] ASTM C260-10-standard specification for air-entraining admixtures for concrete. https://www.astm.org/c0260-10.html. (Accessed 7 July 2024).
[52] Aci PRC-211.1-91: standard practice for selecting proportions for normal, heavyweight, and mass concrete (reapproved 2009). https://www.concrete.org/store/productdetail.aspx?ItemID=211191&Format=DOWNLOAD&Language=English&Units=US_Units. (Accessed 26 August 2023).
[53] Csa A23.1:24/CSA A23.2:24, CSA Group, https://www.csagroup.org/store/product/2701210/. (Accessed 13 February 2025).
[54] ASTM International, ASTM C192/C192m-14 standard practice for making and curing concrete test specimens in the laboratory. https://www.astm.org/c0192_c0192m-14.html. (Accessed 26 August 2023).
[55] e-4574-carbon-dioxide-safety-data-sheet-sds.pdf. https://www.lindecanada.ca/-/media/corporate/praxair-canada/documents-en/safety-data-sheet-linde-canada/e-4574-carbon-dioxide-safety-data-sheet-sds.pdf?la=en-ca. (Accessed 30 August 2024).
[56] C. Pereira, R. Gupta, Exploring the impact of CO2 sequestration on plastic properties, mechanical performance, and microstructure of concrete, Discov Civ Eng 1 (1) (Dec. 2024) 144, https://doi.org/10.1007/s44290-024-00151-2.
[57] S. Monkman, P.A. Kenward, G. Dipple, M. MacDonald, M. Raudsepp, Activation of cement hydration with carbon dioxide, Journal of Sustainable Cement-Based Materials 7 (3) (May 2018) 160–181, https://doi.org/10.1080/21650373.2018.1443854.
[58] CarbonCure-Value-Prop-WP12.pdf. https://www.carboncure.com/wp-content/uploads/2023/05/CarbonCure-Value-Prop-WP12.pdf. (Accessed 20 June 2025).
[59] S. Rashid, M. Singh, An investigation on carbon dioxide incorporated sustainable ready-mix concrete using OPC and PPC, Arabian J. Sci. Eng. 48 (10) (Oct. 2023) 14213–14236, https://doi.org/10.1007/s13369-023-08106-y.
[60] ASTM C39/C39M-21-standard test method for compressive strength of cylindrical concrete specimens. https://www.astm.org/c0039_c0039m-21.html. (Accessed 5 April 2024).
[61] Aashto T 358-19: method of test for surface resistivity indication of concrete's ability to resist chloride ion penetration. https://civilnode.com/download-standard/10672560484310/AASHTO-T-358-19-Method-of-Test-for-Surface-Resistivity-Indication-of-Concrete-s-Ability-to-Resist-Chloride-Ion-Penetration. (Accessed 25 August 2024).
[62] Surf™ | concrete surface resistivity, Giatec Scientific Inc, https://www.giatecscientific.com/products/concrete-ndt-devices/surf-surface-resistivity-meter-giatec/. (Accessed 13 February 2025).
[63] Giatec-SURF-UserManual-2023-07.pdf. https://www.giatecscientific.com/documents/Shared%20Documents/1.0%20External%20Resources/1.11%20Surf/Technical%20support%20resources/User%20Manual/Giatec-SURF-UserManual-2023-07.pdf. (Accessed 15 September 2024).
[64] ASTM C1202-22 standard test method for electrical indication of concrete's ability to resist chloride ion penetration. https://www.astm.org/c1202-22.html. (Accessed 25 August 2024).
[65] Aashto T 277 - standard method of test for electrical indication of concrete's ability to resist chloride ion penetration | GlobalSpec. https://standards.globalspec.com/std/13344840/aashto-t-277. (Accessed 13 February 2025).
[66] Perma™ | rapid chloride permeability, Giatec Scientific Inc, https://www.giatecscientific.com/products/concrete-ndt-devices/perma-rapid-chloride-permeability/. (Accessed 13 February 2025).
[67] Perma2-Manual-Final.pdf. https://www.giatecscientific.com/wp-content/uploads/2013/06/Perma2-Manual-Final.pdf. (Accessed 15 September 2024).
[68] E. Standards, BS EN 12390-8:2019 Testing hardened concrete Depth of penetration of water under pressure. https://www.en-standard.eu. (Accessed 25 August 2024). https://www.en-standard.eu/bs-en-12390-8-2019-testing-hardened-concrete-depth-of-penetration-of-water-under-pressure/.
[69] P. Monteiro, P. Mehta, Concrete: Microstructure, Properties and Materials, 2006.
[70] M. Ibrahim, M. Issa, Evaluation of chloride and water penetration in concrete with cement containing limestone and IPA, Constr. Build. Mater. 129 (Dec. 2016) 278–288, https://doi.org/10.1016/j.conbuildmat.2016.10.085.
[71] ASTM C666-standard test method for resistance of concrete to rapid freezing and thawing. https://www.astm.org/c0666-97.html. (Accessed 15 September 2024).
[72] Elite series freeze thaw cabinet. https://www.humboldtmfg.com/elite-series-freeze-thaw-cabinet.html. (Accessed 13 February 2025).
[73] ASTM C215-19-standard test method for fundamental transverse, longitudinal, and torsional resonant frequencies of concrete specimens. https://www.astm.org/c0215-19.html. (Accessed 15 September 2024).
[74] ASTM C597-22 standard test method for ultrasonic pulse velocity through concrete. https://www.astm.org/c0597-22.html. (Accessed 15 September 2024).
[75] M. Mohana, Assessment of concrete compressive strength by ultrasonic pulse velocity test, Iraqi J. Civil Eng. 14 (1) (2020) 39–46, https://doi.org/10.37650/ijce.2020.172874. https://www.academia.edu/107709346/Assessment_of_concrete_compressive_strength_by_ultrasonic_pulse_velocity_test.
[76] I.A.E. Agency, Guidebook on Non-destructive Testing of Concrete Structures, International Atomic Energy Agency, Text, 2002. https://www.iaea.org/publications/6347/guidebook-on-non-destructive-testing-of-concrete-structures. (Accessed 13 February 2025).
[77] R. Narayan Swamy, Dynamic Poisson's ratio of portland cement paste, mortar and concrete, Cement Concr. Res. 1 (5) (Sep. 1971) 559–583, https://doi.org/10.1016/0008-8846(71)90060-3.
[78] K. Tuutti, Corrosion of Steel in Concrete, Swedish Cement and Concrete Research Institute, Stockholm, 1982. Doctoral Thesis (monograph).
[79] A proposed laboratory method to evaluate the durability of concrete pavement joints against freezing in the presence of deicer salts, Can. J. Civ. Eng. 49 (8) (Apr. 2022) 1351–1365, https://doi.org/10.1139/cjce-2021-0140.
[80] C.S. Rangel, M. Amario, M. Pepe, E. Martinelli, R.D. Toledo Filho, Influence of wetting and drying cycles on physical and mechanical behavior of recycled aggregate concrete, Materials 13 (24) (Dec. 2020) 5675, https://doi.org/10.3390/ma13245675.
[81] iCOR® Archives," Giatec Scientific Inc. Accessed: August. 26, 2024. [Online]. Available: https://www.giatecscientific.com/category/giatec-icor/.
[82] Giatec-iCOR-User-Manual-V-2.0.pdf. https://www.giatecscientific.com/wp-content/uploads/2013/06/Giatec-iCOR-User-Manual-V-2.0.pdf. (Accessed 16 September 2024).
[83] ASTM C876-15-standard test method for corrosion potentials of uncoated reinforcing steel in concrete. https://www.astm.org/c0876-15.html. (Accessed 16 September 2024).
[84] P. Schober, C. Boer, L.A. Schwarte, Correlation coefficients: appropriate use and interpretation, Anesth. Analg. 126 (5) (May 2018) 1763–1768, https://doi.org/10.1213/ANE.0000000000002864.
[85] M. Ali, et al., A review on chloride induced corrosion in reinforced concrete structures: lab and in situ investigation, RSC Adv. 14 (50) (2024) 37252–37271, https://doi.org/10.1039/D4RA05506C.
[86] H. Justnes, M.O. Kim, S. Ng, X. Qian, Methodology of calculating required chloride diffusion coefficient for intended service life as function of concrete cover in reinforced marine structures, Cement Concr. Compos. 73 (Oct. 2016) 316–323, https://doi.org/10.1016/j.cemconcomp.2016.08.006.
[87] D.V. Dinh, Initiation time of corrosion in reinforced concrete structures exposed to chloride in marine environment, Int. J. Civ. Eng. Technol. 8 (9) (Sep. 2017) 9.
[88] ACI 365.1R-00: service-life prediction. https://www.concrete.org/store/productdetail.aspx?ItemID=365100&Format=DOWNLOAD&Language=English&Units=US_AND_METRIC. (Accessed 29 September 2024).
[89] P. Konečný, P. Lehner, T. Ponikiewski, P. Miera, Comparison of chloride diffusion coefficient evaluation based on electrochemical methods, Procedia Eng. 190 (Jan. 2017) 193–198, https://doi.org/10.1016/j.proeng.2017.05.326.